



Effect of Vegetation on the Energy Balance and Evapotranspiration in Tallgrass Prairie: A Paired Study Using the Eddy-Covariance Method

Xiangmin Sun¹ · Chris B. Zou² · Bradford Wilcox¹ · Elaine Stebler²

Received: 14 January 2018 / Accepted: 14 August 2018 / Published online: 25 August 2018
© Springer Nature B.V. 2018

Abstract

We carried out a paired study in tallgrass prairie to evaluate the influence of vegetation on the energy exchange and evapotranspiration. Two eddy-covariance systems were installed over two adjoining sites, one of which was denuded of vegetation, with the adjacent, control site kept undisturbed. Our year-long investigation shows that, for quantifying the ground surface heat flux, the soil heat storage above the soil plates is more important than the sub-surface soil heat flux, both temporally and in magnitude. The incorporation of the soil heat storage, therefore, is indispensable for energy balance closure in areas with short vegetation. At our control site, we observed a critical threshold of $0.17 \text{ m}^3 \text{ m}^{-3}$ in the surface (top 0.3 m) soil water content, whereby the energy partitioning is significantly affected by the presence of the photosynthetically active vegetation when the surface soil water content is higher than this critical threshold. The pattern of energy partitioning approaches that of the treated site when the surface soil water content is lower than this threshold (during drought), because of the suppression of plant physiological activities. This threshold also applies to the surface conductance for water vapour at the control site, where yearly evapotranspiration is $728 \pm 3 \text{ mm}$ (versus $547 \pm 2 \text{ mm}$ for the treated site). Thus, the soil water content and presence of active vegetation are the key determinants of energy partitioning and evapotranspiration. Any land-cover changes or vegetation-management practices that alter these two factors may change the energy and water budgets in tallgrass prairie.

Keywords Eddy covariance · Energy balance · Evapotranspiration · Surface conductance · Tallgrass prairie

✉ Xiangmin Sun
sunxm03@tamu.edu

¹ Department of Ecosystem Science and Management, Texas A&M University, College Station, TX 77843, USA

² Department of Natural Resource Ecology and Management, Oklahoma State University, Stillwater, OK 74078, USA

1 Introduction

Covering 37% of the Earth's surface, the grassland biome is a key component of the terrestrial biosphere, and is crucial for agriculture production, biodiversity conservation, and climate regulation (Boval and Dixon 2012; O'mara 2012). In the Southern Great Plains of the USA, tallgrass prairie is the major type of grassland, especially in the state of Oklahoma (Tyrl et al. 2007), but this prairie is considered a globally endangered resource (Ricketts 1999), with agricultural conversion having consumed all but about 13% of its historical extent (Samson et al. 2004). Recently, this endangered prairie has been threatened by the rapid encroachment of woody plants, particularly juniper (*Juniperus virginiana* L.) (Ge and Zou 2013; Zou et al. 2014), owing mainly to changes in land-use practices that have led to altered fire regimes (McKinley and Blair 2008). Further encroachment by woody plants could substantially affect the water cycle, primarily through altering evapotranspiration (E_T), which is the largest component of the water budget in this region (Zou et al. 2010, 2014). Understanding evapotranspiration and the underlying eco-hydrologic responses of grassland to extreme events in a changing climate, such as during drought, is an essential consideration for studies of ecosystem services, the management of water resources, and the understanding of climate change (Katul et al. 2012).

Energy and water are tightly coupled. A major portion of the incoming solar radiation is converted to sensible (H) and latent heat [LE , where E is evaporation from the surface ($\text{kg m}^{-2} \text{S}^{-1}$) and L is the latent heat of vaporization (J kg^{-1})], which determine the energy exchange and water-vapour flux of the near-surface atmosphere, respectively, and whose partitioning determines many climatological processes and physical properties of the planetary boundary layer, with the latent heat flux also affecting the soil moisture, runoff, and biogeochemical cycles (Wilson and Baldocchi 2000). The most direct method of measuring these vertical turbulent fluxes is through the eddy-covariance (EC) method (Burba 2013), which is widely used in micrometeorology (Baldocchi et al. 2001).

However, the energy imbalance or "closure problem" remains an unsolved problem with the use of the EC method, since the available energy is 10–30% larger than the sum of the latent and sensible heat fluxes in many different vegetation types (Wilson et al. 2002; Foken 2008; Franssen et al. 2010; Foken et al. 2011; Leuning et al. 2012; Anderson and Wang 2014; Masseroni et al. 2014; Russell et al. 2015; Gao et al. 2017; Liu et al. 2017). Correcting for these discrepancies is challenging because many of the involved causes are difficult to quantify (Foken 2008; Foken et al. 2011; Anderson and Wang 2014), including the energy storage (Zuo et al. 2011; Leuning et al. 2012; Russell et al. 2015; Liu et al. 2017), energy advection and mesoscale eddies generated by heterogeneous landscapes (Foken et al. 2011; Stoy et al. 2013; Eder et al. 2015; Gao et al. 2017; Xu et al. 2017), and measurement uncertainties related to sonic anemometers (Kochendorfer et al. 2012; Frank et al. 2013; Horst et al. 2015). For low canopies such as grassland, studies have found that the degree of energy-balance discrepancy differs between sites with high vegetation coverage and those having a greater exposure of soils, owing to the effects of the heat storage in the upper soil layer and the fractional coverage of vegetation (Foken 1998; Oncley et al. 2007; Foken 2008). Yue et al. (2011) reported that, for a semi-arid grassland, integration of the soil heat storage (S_{soil}), which is measured above heat-flux plates, significantly improves the surface-energy balance. In contrast, an analysis on a subset of European FLUXNET stations indicated that the storage terms do not play a major role in the overall closure of the energy balance (Franssen et al. 2010). Given these uncertainties, experiments using two collocated plots, one of them denuded of vegetation, could help disentangle the influences of vegetation and soil heat storage on the closure problem.

The low measurement height and associated relatively small fetch of grassland flux towers facilitate the design of classical, paired ecological experiments, which combine the strength of near-continuous, spatially-integrated, EC monitoring with the explanatory power of causal analysis (Wohlfahrt et al. 2012). With the use of identical equipment on sites having similar land-use histories and nearly identical environmental conditions, confounding factors are minimized, increasing the confidence in the results of different treatments of the vegetation (Ammann et al. 2007; Wohlfahrt et al. 2012). Collocated measurements for contrasting vegetation types in tallgrass prairie include burning versus no burning (Bremer and Ham 1999; Fischer et al. 2012), cultivation versus natural cover (Burba and Verma 2005; Wagle et al. 2016), shrub versus grassland (Novick et al. 2009; Arnold 2010; Scott et al. 2014), and well-watered versus drought conditions (Meyers 2001). The energy balance has been investigated in a boreal jack pine forest with clearcutting versus no treatment (Kidston et al. 2010) but, to our knowledge, no one has experimentally compared treated and untreated sites in grasslands to examine the difference in energy balance. The high variability of precipitation in grasslands and the resultant high intra-annual variations in primary production (Schulze et al. 1994; Knapp and Smith 2001) make these ecosystems a prime setting for the study of ecosystem physiology and evapotranspiration through the experimental manipulation of the vegetation cover (Wever et al. 2002). To accurately quantify the effects of vegetation canopy on surface energy fluxes, the best methodology would be to remove the vegetation from one of two sites, with the second one serving as a control site.

We have selected a pair of collocated tallgrass prairie sites having similar soil, topographic, and vegetation conditions. One site was treated with herbicide and subject to mowing early in the growing season, with the control site left undisturbed. Using one year of continuous EC measurements, we investigated and compared the energy balance, energy partitioning, diurnal and seasonal patterns of evapotranspiration, and the key meteorological or biological factors controlling evapotranspiration for the two sites. Specifically, our objectives were to answer the following questions:

- Influence of the soil heat storage S_{soil} on the energy-balance closure: how do the values of S_{soil} and the sub-surface soil heat flux (G_s as measured by heat-flux plates) compare under two different vegetation coverages? If the value of S_{soil} is integrated into the ground surface heat flux (G_0), does the degree of energy-balance closure differ between the two sites?
- Influence of photosynthetically active vegetation on energy partitioning: how different are the seasonal and diurnal patterns of energy partitioning between the two sites, owing to the presence of active vegetation at the control site and its absence at the treated site?
- Evapotranspiration variation and the key controlling factors: how does evapotranspiration vary, temporally and in magnitude, under contrasting vegetation coverages? How does the cumulative evapotranspiration compare with the precipitation? Does the difference in vegetation cover between the paired sites translate to a difference in controlling factors for evapotranspiration?

2 Description of Study Sites

The study was conducted at the Range Research Station (36° 03' 24.6''N, 97° 11' 28.3''W, elevation about 330 m above sea level), which is a research and extension facility administered by the Oklahoma Agricultural Experiment Station, Oklahoma State University, and is located about 11 km south-west of Stillwater in Payne County, Oklahoma, USA. The terrain is

mostly flat, with slopes of 3–8%, and the soil type is mainly Stephenville–Darnell complex (Soil Survey Staff 2003). This tallgrass prairie is dominated by perennial, warm-season (C_4) grasses, including little bluestem (*Schizachyrium scoparium* [Michx.] Nash), big bluestem (*Andropogon gerardii* Vitman), Indiangrass (*Sorghastrum nutans* [L.] Nash), switchgrass (*Panicum virgatum* L.), and tall dropseed (*Sporobolus asper* [Michx.] Kunth) (Limb et al. 2010). According to Mesonet long-term average climate data (2002–2015), this site has a sub-humid climate with an average air temperature of 15.5 °C, a mean annual precipitation of 852 mm, an average wind speed of 4 m s⁻¹ (maximum gusts of 7.6 m s⁻¹), an average relative humidity of 66%, an average atmospheric pressure of 97.7 kPa, an average daily global radiation of 192 W m⁻², and an average daily net radiation of 98 W m⁻² (Brock et al. 1995; McPherson et al. 2007; Mesonet 2016).

3 Materials and Methods

From 2014–2015, two EC towers separated by a distance of 250 m were installed in the Range Research Station, with one in the north of the grassland tract, and the other in the south. In 2016, we delineated two collocated experimental sites, with one surrounding the northern EC tower, and the other surrounding the southern tower (Fig. 1). The northern site was sprayed with herbicide on 12 May 2016, mowed on 29 May (a large amount of the remaining cover of dried standing stems was left, so that little bare ground was visible), and again sprayed with herbicide on 20 July. Having been thus treated for vegetation removal, this site is hereafter referred to as Site T. The southern site was left as natural, undisturbed grassland, to serve as a control, and thus is hereafter referred to as Site C. At each of the two sites, the EC tower was located at the north-western or northern end, facing the greatest fetch as determined by the prevailing wind direction (south or south–south-east; see Appendix 1, Fig. 11).

3.1 Eddy-Covariance Systems and Biometeorological Sensors

Each EC tower was equipped with an integrated CO₂ and H₂O open-path gas analyzer and three-dimensional sonic anemometer (EC100, IRGASON, Campbell Scientific Inc., Logan, Utah) mounted 3 m above the ground. A standard set of sensors for measuring biometeorological variables was also installed at each tower, including two heat-flux plates (HFP01, Hukseflux, Delft, Netherlands) set 0.08 m below the ground, one averaging soil thermocouple (TCAV, Campbell Scientific Inc., Logan, Utah), with the two members of each pair set at 0.02 m and 0.06 m below the ground, with a distance of 1 m between the two pairs, one water-content reflectometer (CS616, Campbell Scientific Inc., Logan, Utah) set 0.025 m below the ground, a net radiometer (NR-Lite2, Kipp and Zonen, Delft, Netherlands), and a temperature probe for the ambient air (107, Campbell Scientific Inc., Logan, Utah) with a solar radiation shield. All the biometeorological sensors sampled every 5 s, and 30-min averages were calculated and stored with a datalogger (CR3000, Campbell Scientific Inc., Logan, Utah). To measure the normalized difference vegetation (NDV) index, we installed spectral reflectance sensors (SRS, Decagon Inc., Pullman, Washington) in close proximity to the two EC towers. The pair mounted Site T was operational only for 24 days (12 May to 4 June) following the initial herbicide spraying, while the other pair, in Site C, was operational beginning in February. A rain gauge (HOBO RG3, Onset Inc., Bourne, Massachusetts) was mounted above the canopy at Site C to record precipitation (precipitation events were assumed to be the same for both sites). Finally, soil-moisture probes (ECH₂O EC-5, Decagon,

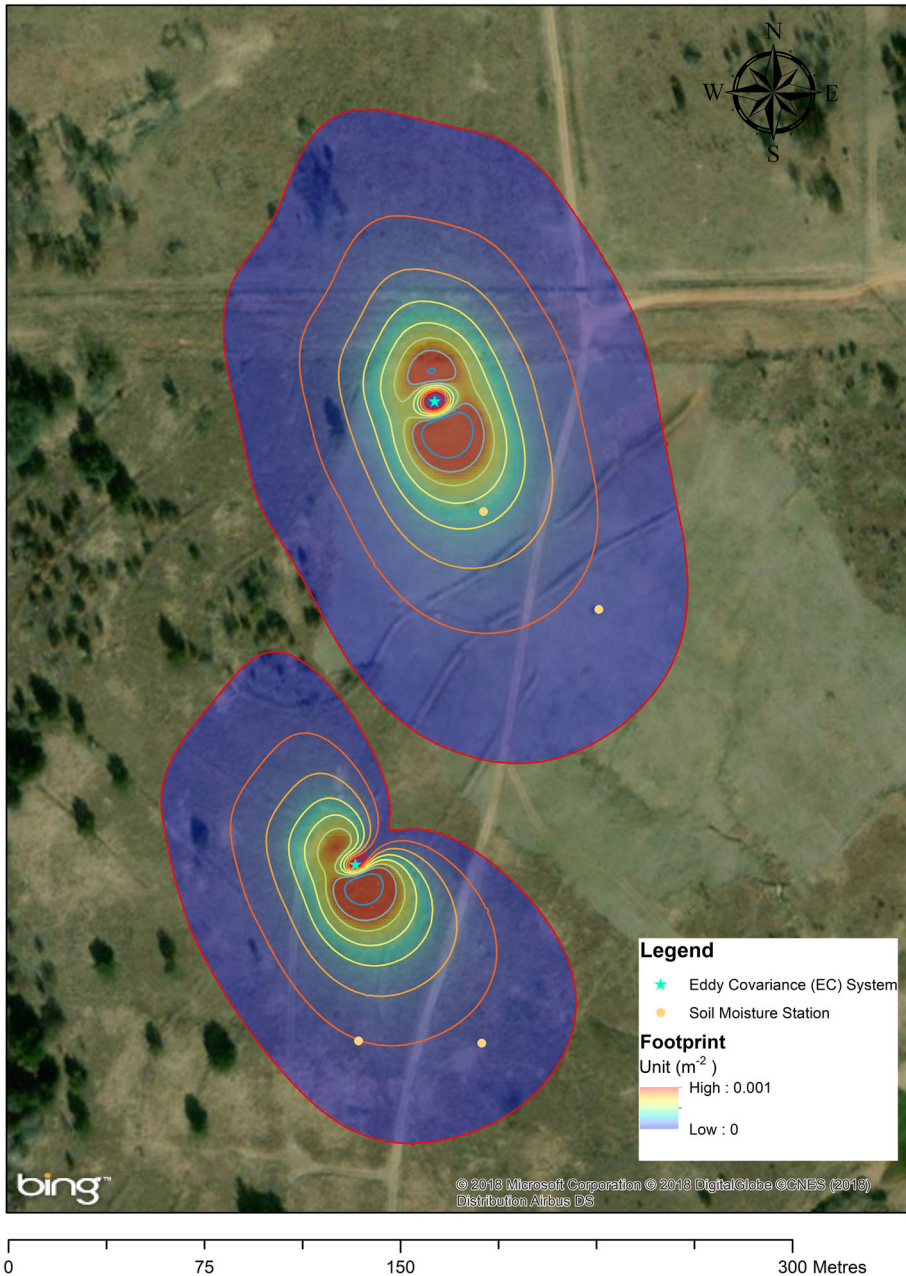


Fig. 1 Configuration of the study sites with superimpositions of the flux-footprint climatology. Except for the space immediately surrounding each EC tower, the contour lines from inner to outer are the yearly cumulative footprint climatology boundaries from 10 to 80%, with an interval of 10%. The EC devices were mounted 3 m above the ground

Pullman, Washington) were inserted at two soil-moisture stations at each site at depths of 0.05, 0.2, 0.45, and 0.8 m, to measure the volumetric soil water content (θ) of four depth intervals across the soil profile: 0–0.1 m, 0.1–0.3 m, 0.3–0.6 m, and 0.6–1.0 m (Fig. 1). All the measurements described above were recorded in terms of the local time ($LT = UTC - 6$ h; no daylight saving time).

Surface turbulent-flux measurements were collected at a frequency of 10 Hz, and computed for an average of 30 min with biometeorological data via the EddyPro software (version 6.2.1, LI-COR Biosciences, Lincoln, Nebraska). We adopted the observational results from Conant and Risser (1974) for dynamic canopy heights. The key processing steps included despiking and the statistical screening of raw data (Vickers and Mahrt 1997), tilt correction with the double rotation method (Wilczak et al. 2001), spectral corrections (Moncrieff et al. 1997; Foken et al. 2004; Moncrieff et al. 2005), and the compensation for density fluctuations (Webb et al. 1980). Subsequently, EddyPro quality flags were calculated for all fluxes on the basis of the steady state test and the test for developed turbulent conditions, and combined into a 0–1–2 system (Mauder and Foken 2006).

3.2 Footprint Analysis, Quality Control, and Gap Filling

To determine whether the flux footprints of the two sites overlapped spatially, we estimated the climatology boundaries of the two-dimensional footprint with yearly cumulative contributions from 10 to 80% (with an interval of 10%) to the measured turbulent fluxes (Fig. 1). We used the Flux Footprint Prediction model (Kljun et al. 2015) for these estimates, because of its ability to accurately predict the maximum footprint boundary (Heidbach et al. 2017). The planetary boundary-layer height, which is used by the Flux Footprint Prediction model for crosswind-integrated scaling, was obtained from the North American Regional Reanalysis data provided by the National Oceanic and Atmospheric Administration's Physical Sciences Division, Boulder, Colorado, USA (<https://www.esrl.noaa.gov/psd/>). The sample code employed for extracting time series of the planetary boundary-layer height based on the geographical location is provided in Appendix 2. As for the footprint analysis, we calculated two matrices along the wind direction (Kljun et al. 2004): X_i ($i = 10\text{--}90\%$, with an interval of 20%), provided by the along-wind distance contributing i cumulative turbulent fluxes, and X_{peak} , which is the upwind distance providing the highest contribution. Fetches extending beyond the boundaries of the two sites (as defined by the $X_{70\%}$ footprint criterion) were discarded after the first treatment (12 May 2016). Following footprint filtering, the median $X_{70\%}$ and X_{peak} were 92.5 and 48.6 m for Site T, and 88.9 and 39.2 m for Site C.

The EC results produced by the EddyPro software were subject to further filtering and quality testing. Under conditions of stable stratification and low turbulent mixing (primarily during the night), a routine filtering criterion for the friction velocity u_* was applied on a monthly basis (with thresholds ranging between 0.06 and 0.18 m s^{-1} for Site T, and between 0.09 and 0.25 m s^{-1} for Site C) via the moving-point test (Papale et al. 2006). Poor-quality data (those having quality flags = 2) and outliers (values beyond three times of the standard deviations) were screened for values of the sensible and latent heat fluxes. The FREddyPro package (<https://cran.r-project.org/web/packages/FREddyPro/index.html>) was employed for all despiking, the filtering of monthly u_* , and other general post-processing of EddyPro output files.

After all the filtering operations, data coverage for the remaining 30-min sensible and latent heat fluxes are 55.3 and 46.5%, respectively, for Site T, and 72.6 and 59.5%, respectively, for Site C. Gap-filling (Reichstein et al. 2005; Wutzler et al. 2018) was implemented

with the R package REdyProc developed at the Max Planck Institute of Biogeochemistry (<https://www.bgc-jena.mpg.de/bgi/index.php/Services/REdyProcWebRPackage>). Records of ancillary environmental factors, such as global radiation and air temperature, were used to separately fill gaps in the time series of the sensible and latent heat fluxes via the default routines of the “gap filling algorithm after u_* filtering within seasons,” with the u_* thresholds based on 50% of the bootstrap re-sampling. Bowen ratios calculated during the night (for global radiation $< 20 \text{ W m}^{-2}$) were filtered, and Bowen-ratio outliers during the daytime were removed (outside the range -5 to 15 , which accounted for less than 1% at each site), and then filled by the linear method (Moritz et al. 2015) with the “imputeTS” package (<https://cran.r-project.org/web/packages/imputeTS/index.html>).

Uncertainties in sensible and latent heat fluxes were integrated from 30-min random errors of fluxes as in Finkelstein and Sims (2001), including the errors in gap-filling estimates. The uncertainty in the 30-min evapotranspiration propagates from that in the 30-min latent heat flux, and uncertainties in yearly budgets and monthly averaged values of evapotranspiration were calculated by integrating the additive variance of random measurement errors and gap-filling uncertainties. We present aggregated uncertainty estimates with 95% confidence intervals.

3.3 Energy-Balance Closure

Whether the EC method has underestimated the surface turbulent fluxes is usually assessed by checking the energy-balance closure (Wilson et al. 2002; Kosugi et al. 2007). As shown in Fig. 2, the surface energy budget can be formulated as

$$R_n - G_0 - S_{above} = LE + H + A_d, \quad (1)$$

with all terms having units of W m^{-2} , where R_n is the net radiation (the balance between incoming global radiation and outgoing reflection and thermal radiation), S_{above} is the above-ground heat storage, consisting of heat stored in the above-ground biomass and photosynthetic heat storage flux, A_d is the advective heat flux beneath the EC sensors and E_T the kinematic moisture flux due to evaporation, G_0 is the ground surface heat flux, consisting of sub-surface heat flux (G_s) measured by heat-flux plates at a depth of 0.08 m here, and the soil heat storage (S_{soil}) above the plates (Meyers and Hollinger 2004),

$$S_{soil} = \frac{\Delta T_s C_s d}{t}, \quad (2)$$

where ΔT_s is the change in soil temperature above the fixed depth d (0.08 m) during the measuring time interval t (30 min), and C_s is the heat capacity of moist soil ($\text{J kg}^{-1} \text{K}^{-1}$). More details on the value of C_s can be found in Campbell Scientific (2016).

In calculating the energy-balance closure, we have omitted the above-ground heat storage because, in the case of a low vegetation canopy, the magnitude of the photosynthetic flux is small (Twine et al. 2000), and the storage in the above-ground biomass is insignificant (Wilson et al. 2002). Advection was omitted as well, not only because it is considered to be insignificant over flat terrain (Baldocchi 2003), but also because its direct measurement is technically challenging (Papale et al. 2006; Foken et al. 2011). Thus, the calculation of the energy balance (at yearly and monthly scales) involves the linear regression between the instantaneous turbulent-flux measurements ($H + LE$ [before gap-filling]) from the EC method, and the mea-

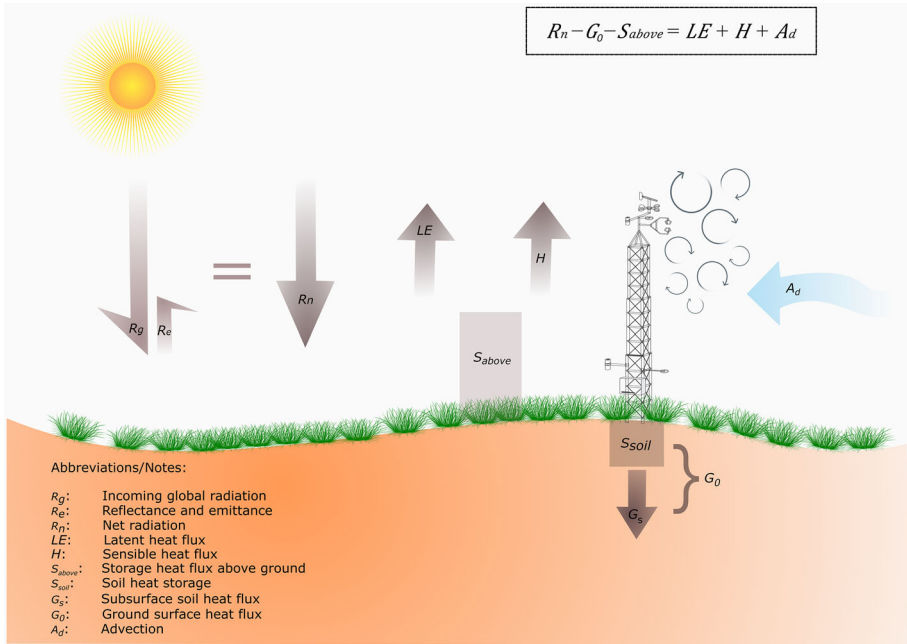


Fig. 2 Diagram of surface-energy budget and energy-balance closure. The net radiation (R_n) is the source of all energy fluxes within the boundary layer, including the latent heat flux (LE) consumed in the process of evapotranspiration (ET), the sensible heat flux (H) associated with temperature variations, the ground surface heat flux (G_0), consisting of the soil heat storage above the heat-flux plate (S_{soil}) and the sub-surface soil heat flux at the measurement depth (G_s), the above-ground heat storage (S_{above}), and the advective heat flux from all directions (A_d)

measurements of the available energy ($R_n - G_0$) from the independent biometeorological sensors, assuming

$$R_n - G_0 = LE + H. \tag{3}$$

Lastly, we coerced the energy-balance closure using the Bowen ratio method (Twine et al. 2000).

3.4 Parametrization of the Bulk Surface Characteristics

To interpret the influence of meteorological and biological factors on the evapotranspiration variations, we calculated the surface conductance to water vapour (g_s , $m\ s^{-1}$) during daytime periods (for global radiation $> 20\ W\ m^{-2}$) based on the inversion of the Penman–Monteith equation (Monteith 1965),

$$g_s = \frac{g_a}{\frac{\Delta(R_n - G) + \rho_a c_p VPD g_a}{\gamma LE} - \frac{\Delta}{\gamma} - 1}, \tag{4}$$

where g_a is the aerodynamic conductance of the air layer between the canopy top and the measurement height ($m\ s^{-1}$, described below), Δ is the slope of the saturation vapour pressure versus air temperature ($kPa\ K^{-1}$), ρ_a is the air density ($kg\ m^{-3}$), c_p is the specific air heat capacity at constant pressure ($J\ kg^{-1}\ K^{-1}$), VPD is the vapour pressure deficit (kPa), and γ is

the psychrometric constant (kPa K^{-1} , in terms of vapour pressure and not specific humidity as is traditional in micrometeorology),

$$\gamma = 0.665 \times 10^{-3} P, \quad (5)$$

where P is the atmospheric pressure (kPa). The aerodynamic conductance g_a (m s^{-1}) is defined as

$$\frac{1}{g_a} = \frac{u}{\mu_*^2} + 6.2\mu_*^{-0.67}, \quad (6)$$

where u is the wind speed (Monteith and Unsworth 2013). Leaf stomata and soil spaces are the major paths for surface water-vapour conductance, and thus the value of g_s is proportional to the leaf area index or the NDV index and water-vapour conductance through the soil profile. The main factors controlling the value of g_a are the surface characteristics and the wind speed u .

The Penman–Monteith model (Monteith and Unsworth 2013) includes the effects of surface resistance ($r_s = g_s^{-1}$) and the above-canopy aerodynamic resistance ($r_a = g_a^{-1}$) on the potential evapotranspiration,

$$LE = \frac{\Delta(R_n - G) + \frac{\rho c_p VPD}{r_a}}{\Delta + \gamma \left(1 + \frac{r_s}{r_a}\right)}. \quad (7)$$

As $r_a \rightarrow \infty$ or zero, the latent heat flux can be converted to either the equilibrium latent heat flux (LE_{eq}) or the imposed latent heat flux (LE_{im}) (Jarvis and McNaughton 1986), which implies that the Penman–Monteith equation can be transformed as

$$LE = \Omega LE_{eq} + (1 - \Omega)LE_{im}, \quad (8)$$

where Ω is the decoupling factor,

$$\Omega = \frac{(\Delta + \gamma)}{\Delta + \gamma \left(1 + \frac{g_a}{g_s}\right)}. \quad (9)$$

These calculations show that the latent heat flux lies between the two limits defined by the values of LE_{eq} and LE_{im} . When the energy budget is dominated by a diabatic process or available energy, the value of Ω approaches unity, so that the evapotranspiration rate is then effectively independent of the value of g_s and the vapour pressure deficit VPD , and may thus be viewed as decoupled from the prevailing weather conditions (Monteith and Unsworth 2013). Conversely, the decoupling factor Ω approaches zero when the evapotranspiration is controlled by surface conductance for water vapour g_s and the vapour pressure deficit VPD , indicating greater coupling between the surface and near-surface atmosphere.

4 Results

4.1 Comparison of Environmental Conditions

While our paired adjacent sites exhibited similar meteorological conditions in general, there were differences in the net radiation and wind speed. Total rainfall for the year was 721 mm, amounting to 85% of the 15-year mean (Mesonet 2016), with 604 mm (84%) received during the growing season (April through October). However, during those months there were several

dry intervals, including 1–17 June and 1–24 August with rainfall < 10 mm (Fig. 3a). In late May (about 1 week after the first herbicide application to Site T), the daily mean R_n began to diverge between the two sites. The difference in daily mean R_n for the period June–October was $13 \pm 1 \text{ W m}^{-2}$ (Fig. 3b), where, unless explicitly stated otherwise, mean values are expressed as \pm the 95% confidence interval hereafter. The daily mean air temperature T_{air} and the vapour pressure deficit VPD at the two sites were nearly identical, and showed the same seasonal patterns, reflecting the general seasonal pattern in the value of R_n (Fig. 3c, e). The yearly mean wind speed was 3.0 m s^{-1} at Site T and 2.7 m s^{-1} at Site C. After herbicide application at Site T, the NDV index plummeted from 0.6 to 0.3 over the 24-day measurement period, whereas the NDV index at Site C varied in response to the natural leaf development (Fig. 3f). The vegetation removal resulted in a decrease in the value of u_* at Site T during the period June to October to 0.25 m s^{-1} (versus 0.28 m s^{-1} at Site C; data not shown).

Before the herbicide application, soil–water dynamics across the profile (except for the lowest depth interval) were similar for the two sites, with a substantial divergence in soil water content θ gradually developing following the treatment. The surface and near-surface soils (to a depth of 0.3 m) at both sites exhibited marked and prompt responses to the precipitation inputs, but varied over different ranges during the greater part of the growing season. As the depth increased, these sensitive responses gradually flattened, and the divergence in the values of θ between the two sites progressively developed in these deeper layers until the heaviest rainfall (81 mm on 6 October) when the discrepancy basically vanished (see Appendix 1, Fig. 12).

4.2 Footprint Climatology

The yearly flux-footprint climatology and contour lines (10–80% with an interval of 10%) show that the flux footprints of the two EC measurements do not overlap (Fig. 1), with the nearest separation of the outer boundaries (80% climatology lines) approximately 10 m. The spatial patterns of these footprints were in line with the prevailing wind directions (see Appendix 1, Fig. 11). The flux footprint of the EC tower of Site T was larger than its counterpart at Site C, coinciding with Site T's comparatively higher wind speed and lower u_* .

4.3 Ground Surface Heat Flux and Energy Balance

The diurnal pattern of ground surface heat flux G_0 has a greater seasonal variation due to the greater difference in the soil heat storage S_{soil} rather than the sub-surface heat flux G_s between our sites (Fig. 4). The difference in the value of S_{soil} between the two sites was significant at midday in spring (21 March–20 June), summer (21 June–20 September), and winter (21 December–20 March), while diurnal peaks in the values of S_{soil} varied within narrow ranges at Site T, between $55 \pm 5 \text{ W m}^{-2}$ (at 1100 LT in spring) and $42 \pm 3 \text{ W m}^{-2}$ (at 1200 LT in summer), but varied dramatically at Site C, between $88 \pm 8 \text{ W m}^{-2}$ (at 1130 LT in spring) and $45 \pm 5 \text{ W m}^{-2}$ (at 1200 LT in autumn; 21 September–20 December). Diurnal patterns of the sub-surface heat flux were subdued at both sites, and thus comparable under the dry residual vegetation at one site, and an active canopy at the other. Both sites exhibited a substantial phase lag between the soil heat storage (upper 0.08 m of the profile) and sub-surface heat flux (depths below 0.08 m), but this lag was especially pronounced at Site T, where the value of S_{soil} peaked between 1100 and 1200 LT, while the values of G_s peaked between 1430 and

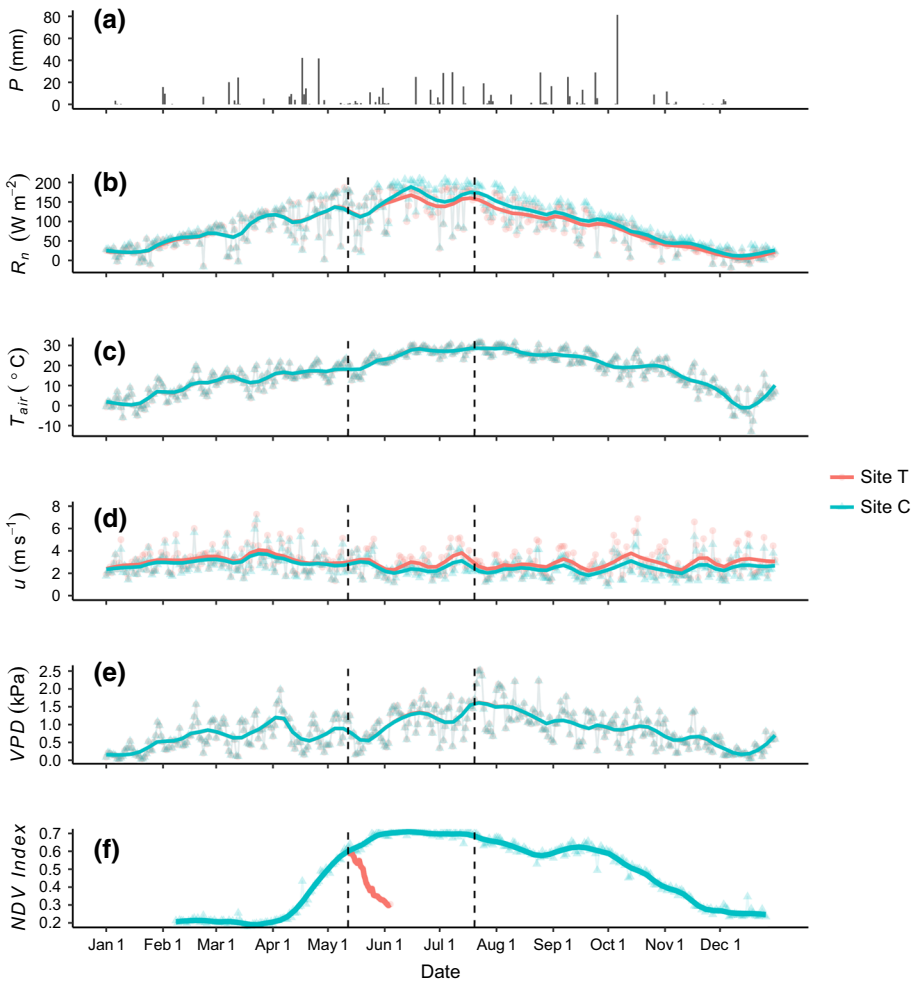


Fig. 3 Seasonal variations in relevant environmental factors for the two experimental sites. These environmental factors are daily precipitation sum (a) and daily mean values of net radiation (b), air temperature (c), wind speed (d), vapour pressure deficit (e), and NDV index (f) for the two sites. Each vertical bar in a represents the daily total precipitation; each point in b–e represents the daily mean value observed over a 24-h period; each point in f represents the mean NDV index between 1200 and 1400 LT. The smoothed curves are fitted via locally weighted regression with a span of 0.1. The two dashed vertical lines represent the dates of the herbicide application to Site T (12 May and 20 July 2016)

1530 LT (see Appendix 1, Fig. 13). The greater magnitudes and more marked variation in the value of S_{soil} show the importance of its role in quantifying ground surface heat flux G_0 , both temporally and in magnitude.

Taking the value of S_{soil} into account, the slope of the energy-balance regression is 0.83 for Site T and 0.86 for Site C (Fig. 5), implying the measured surface turbulent fluxes are approximately 15% lower than the available energy for both sites. The monthly series of the energy-closure slopes are found to be different between the two sites (paired t test, p value < 0.01, Table 1), with the energy balance typically lower, and intercepts typically higher at Site T, where wind speeds were usually greater, and the friction velocity was lower

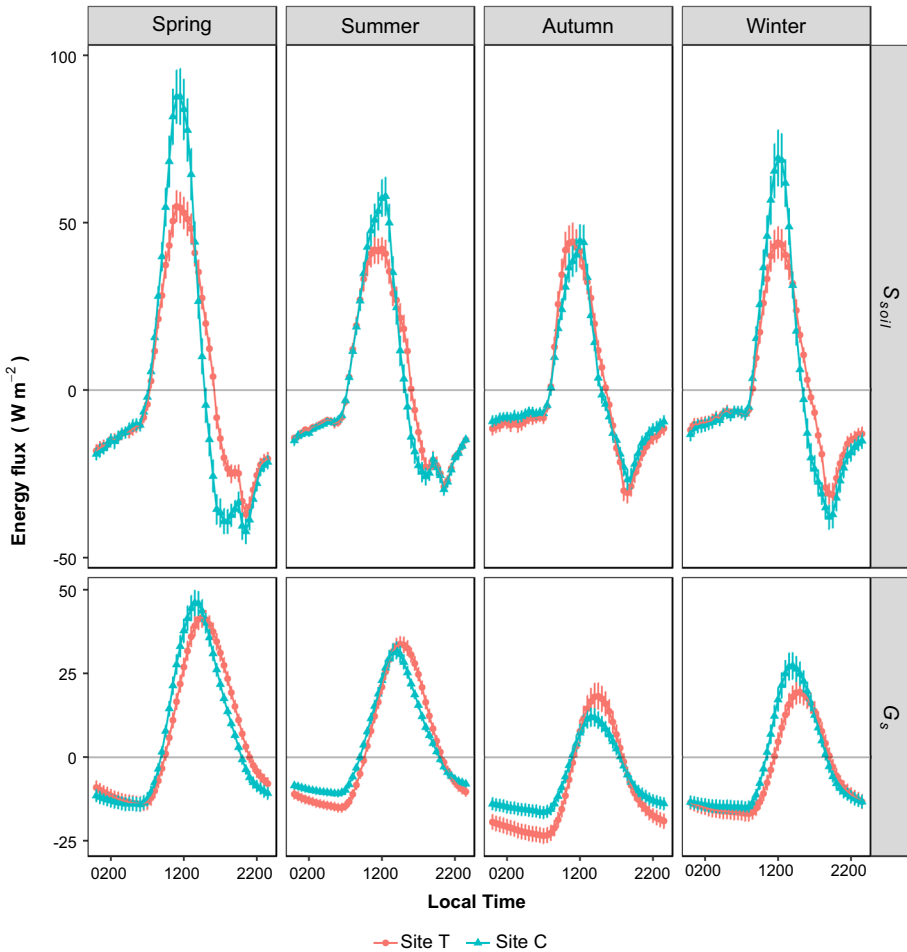


Fig. 4 Diurnal variations of the two components of ground surface heat flux (G_0)— S_{soil} , in the upper 0.08 m of the soil profile, and G_s , in the deeper levels—for the two sites during the four seasons, defined according to the amount of solar radiation received: spring (21 March–20 June), summer (21 June–20 September), autumn (21 September–20 December), and winter (21 December–20 March). Each point is a 30-min ensemble mean for its corresponding flux during that entire season, with a 95% confidence interval. Negative values represent upwards diffusion of heat lost from the surface, and positive values represent downwards absorption through the ground

as a result of the herbicide treatment (see Figs. 3b, 5). The energy balance weakened during the growing season at Site C when the photosynthesis activity and energy storage within and under the developed vegetation canopy, namely the above-ground heat storage, probably enhanced to a non-negligible amount (Table 1).

4.4 Energy Partitioning under Contrasting Types of Vegetation Cover

After the vegetation removal, the net radiation R_n became lower at Site T than at Site C (see Fig. 6, summer and autumn graphics), but the timing of the diurnal peak values of R_n of

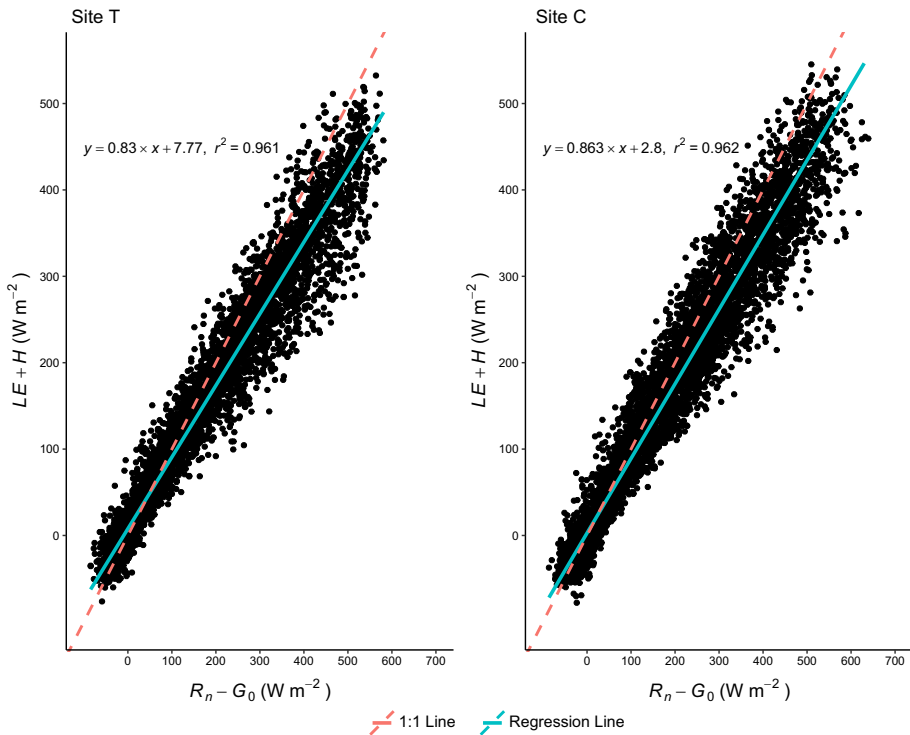


Fig. 5 Scatter plots of the measured half-hourly series of available energy ($R_n - G_0$) versus the sum of the turbulent fluxes ($H + LE$) for the two sites. The solid line (teal) represents the best linear regression. The numbers of data points are 7026 for Site T and 9133 for Site C

the two sites is similar (1230 LT during summer and autumn, and 1300 LT during winter and spring). The diurnal patterns of the ground surface heat flux G_0 has a greater seasonal fluctuation at Site C than at Site T (Fig. 6), which agrees with the seasonal difference in S_{soil} between the two sites (Fig. 4). At both sites, the diurnal patterns of G_0 are mainly controlled by the diurnal patterns of S_{soil} , which in turn is mainly controlled by the diurnal patterns in the value of ΔT_s (data not shown). The generally higher midday magnitude of G_0 at Site C compared with Site T is in accordance with the contrast in the values of R_n between the two sites. When the value of S_{soil} is taken into consideration, the diurnal patterns of G_0 and R_n become largely synchronous, with phase shifts usually occurring within 30 min.

As shown in Fig. 6, the patterns of energy partitioning of the sensible and latent heat fluxes for the diurnal processes at the two sites are generally comparable in the autumn and winter (largely matching the non-growing season), but are dramatically different in spring and summer (roughly the growing season), especially during the early afternoon (1200–1400 LT) when the sensible heat flux is consistently higher at Site T, whereas the latent heat flux is higher at Site C. A difference in the energy partitioning at the seasonal scale is also evident in the monthly values (see Appendix 1, Fig. 14). During the peak growing season, (June–July), average early-afternoon sensible and latent heat fluxes at Site C were 133 ± 6 and 280 ± 8 $W m^{-2}$, respectively, and 246 ± 10 and 173 ± 5 $W m^{-2}$, respectively, at Site T. These differences in energy partitioning are mirrored by the sensible and latent heat fluxes normalized by the available energy at the daily temporal resolution (see Appendix 1, Fig. 15).

Table 1 Monthly linear regression coefficients (slope and intercept) between the available energy ($R_n - G_0$) and surface energy fluxes ($H + LE$) for Site T and Site C

Month	Slope		Intercept		R^2	
	Site T	Site C	Site T	Site C	Site T	Site C
Jan	0.814	0.920	2.96	3.23	0.951	0.967
Feb	0.821	0.927	3.63	-2.15	0.959	0.937
Mar	0.792	0.923	5.02	-1.00	0.943	0.940
Apr	0.820	0.861	6.75	1.49	0.952	0.942
May	0.856	0.865	6.37	2.28	0.953	0.953
Jun	0.871	0.841	16.4	0.83	0.961	0.972
Jul	0.823	0.866	14.0	4.08	0.975	0.976
Aug	0.822	0.860	13.3	2.77	0.965	0.969
Sep	0.835	0.866	11.9	2.49	0.969	0.969
Oct	0.847	0.897	7.53	2.34	0.966	0.974
Nov	0.818	0.879	8.17	3.58	0.965	0.968
Dec	0.823	0.914	3.55	5.12	0.945	0.958
Yearly	0.830	0.863	7.77	2.80	0.961	0.962

Thus, the increase in the sensible heat flux that resulted from the vegetation treatment at Site T triggered a rise in the Bowen ratio (H/LE , which is a measure of energy partitioning) during the major part of the growing season.

Together with the greater magnitude of the latent heat flux, the soil water content θ at Site C is severely depleted across the profile (see Fig. 7; Fig. 12 in Appendix 1), especially within the upper 0.3 m ($\theta_{0.3}$) where there is large evaporation from the surface layer, as well as water loss in the lower portions through uptake by roots (transpiration). The depletion of $\theta_{0.3}$ below a critical threshold ($0.17 \text{ m}^3 \text{ m}^{-3}$) at Site C during the height of the drought in the period 13–24 August led to a suppression of plant transpiration, which in turn caused a convergence in the pattern of energy partitioning between the two sites. Namely, once the value of $\theta_{0.3}$ fell below this critical threshold, plant physiological activities became under severe drought stress, and thus the normalized latent heat flux and the Bowen ratio at Site C approached the concurrent average values at Site T (see Fig. 15 in Appendix 1).

4.5 Seasonal and Diurnal Variations in Evapotranspiration

The evapotranspiration exhibits a clear seasonal pattern at both sites, attaining its maximum values during the peak growing season, and generally dropping below 1 mm day^{-1} during the winter (Fig. 7). Following the vegetation treatment, the daily evapotranspiration at Site T was typically much lower than at Site C, with the peak daily evapotranspiration at Site T approaching 3.5 mm day^{-1} on 10 July, but reaching close to 5 mm day^{-1} from mid-June to nearly the end of July at Site C. Figure 8 shows that the daytime evapotranspiration was significantly lower at Site T than at Site C from May to September, which is particularly noticeable around midday (1200–1400 LT) during the peak growing season, when evapotranspiration averaged $0.11 \text{ mm (30 min)}^{-1}$ at Site T versus $0.18 \text{ mm (30 min)}^{-1}$ at Site C.

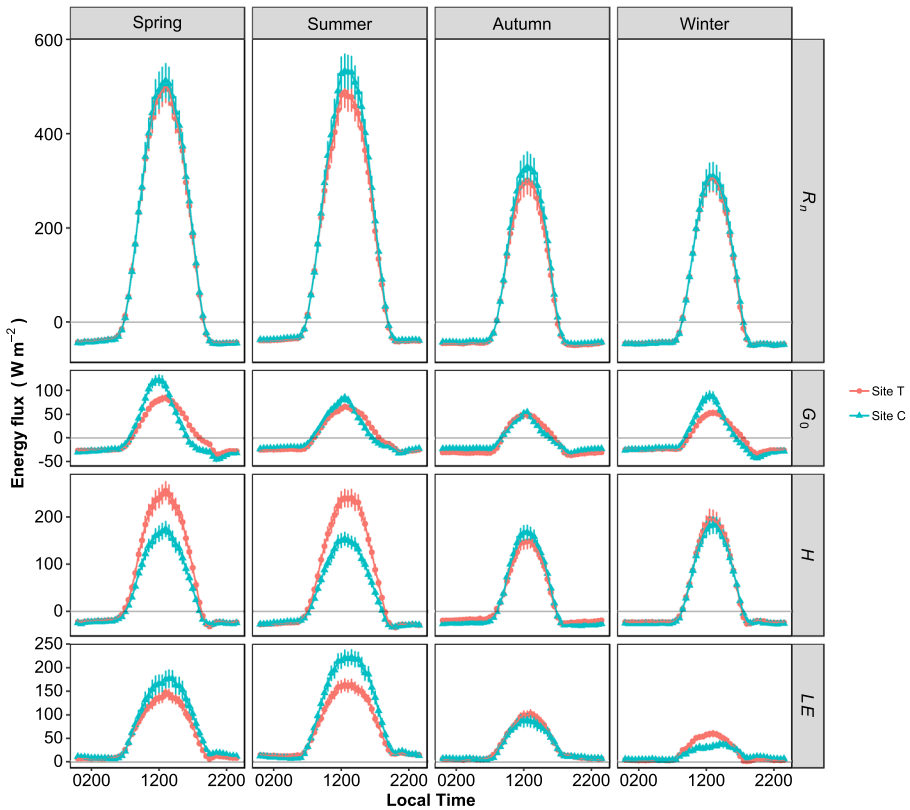


Fig. 6 Diurnal patterns of energy partitioning for the two sites during the different seasons. Each point represents the ensemble mean value of that energy component during the season, with a 95% confidence interval. The sign of the energy fluxes (R_n and G_0) is positive when moving downwards into the ground, while that of the surface turbulent fluxes (H and LE) is positive when directed from the ground towards the atmosphere

The cumulative evapotranspiration readings for the paired sites were similar prior to treatment, and diverged substantially afterwards (Fig. 9). At Site T, the cumulative evapotranspiration remained consistently lower than the cumulative precipitation from early March, while the cumulative evapotranspiration at Site C began to exceed the cumulative precipitation on 21 July, reaching 429 ± 2 mm, and remaining so until the heaviest daily rain on 6 October. The yearly cumulative evapotranspiration for Site C is 728 ± 3 mm, which is about 181 mm higher than for Site T (547 ± 2 mm), and was close to the yearly precipitation (721 mm). For Site T, the absence of active vegetation since early in the growing season resulted in a 25% drop in yearly evapotranspiration.

4.6 Bulk Surface Parameters and the Vegetation Index

Differences in bulk surface parameters between the two sites reveal that different factors control the seasonal variations of the evapotranspiration (Fig. 10). The aerodynamic conductance above the canopy g_a was generally lower at Site T (yearly mean of 27 ± 1 mm s⁻¹) than at Site C (yearly mean of 34 ± 1 mm s⁻¹), which is consistent with the higher u values

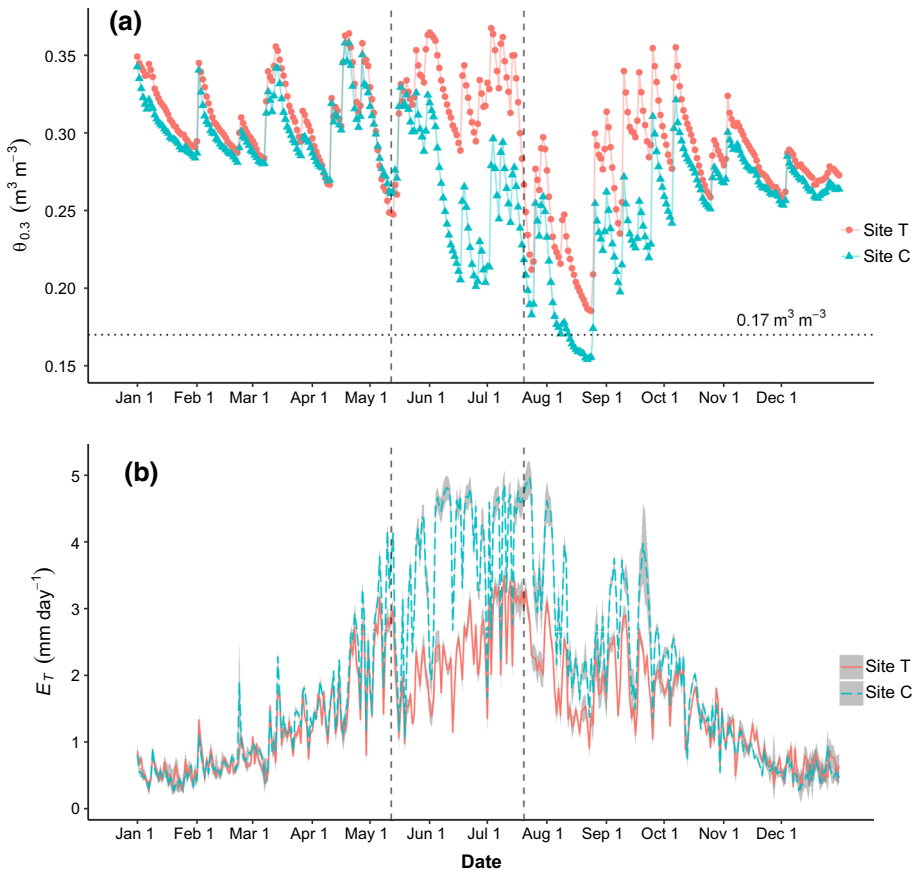


Fig. 7 Contrasts in soil water content of the upper 0.3 m ($\theta_{0.3}$, **a**) and daily evapotranspiration (**b**) between the two sites. The lines for the daily evapotranspiration represent sums of 30-min evapotranspiration data from either the measurements or gap-filling in that day, surrounded by the 95% confidence interval (grey shaded ribbons) derived from the uncertainty analysis in the random sampling and gap-filling. The two vertical dashed lines represent the dates of herbicide application. The horizontal dotted line represents the $\theta_{0.3}$ threshold at which a change in the pattern of energy partitioning is triggered

and lower u_* values at Site T than at Site C (see Eq. 6), with this difference not substantially influenced by the vegetation removal. However, the surface conductance g_s , which was similar at the two sites before the treatment, diverged substantially afterwards. From June to October, the mean values of g_s were $8 \pm 1 \text{ mm s}^{-1}$ at Site T and $22 \pm 2 \text{ mm s}^{-1}$ at Site C. Except for some periods during the first half of the growing season (mainly in May and June) at Site C, the value of g_s was generally less than the value of g_a for both sites, with the result that the evapotranspiration fluxes were more constrained by the surface conductance than by the aerodynamic conductance. Consequently, during the greater part of the growing season following treatment, the decoupling factor Ω was usually lower at Site T than at Site C—especially during the peak growing season when the mean value of Ω was 0.5 and 0.8 at Site T and Site C, respectively. Thus, during the greater part of the growing season, the evapotranspiration at Site T was more coupled with the meteorological conditions and controlled by the abiotic factors (the surface conductance and vapour pressure deficit), whereas

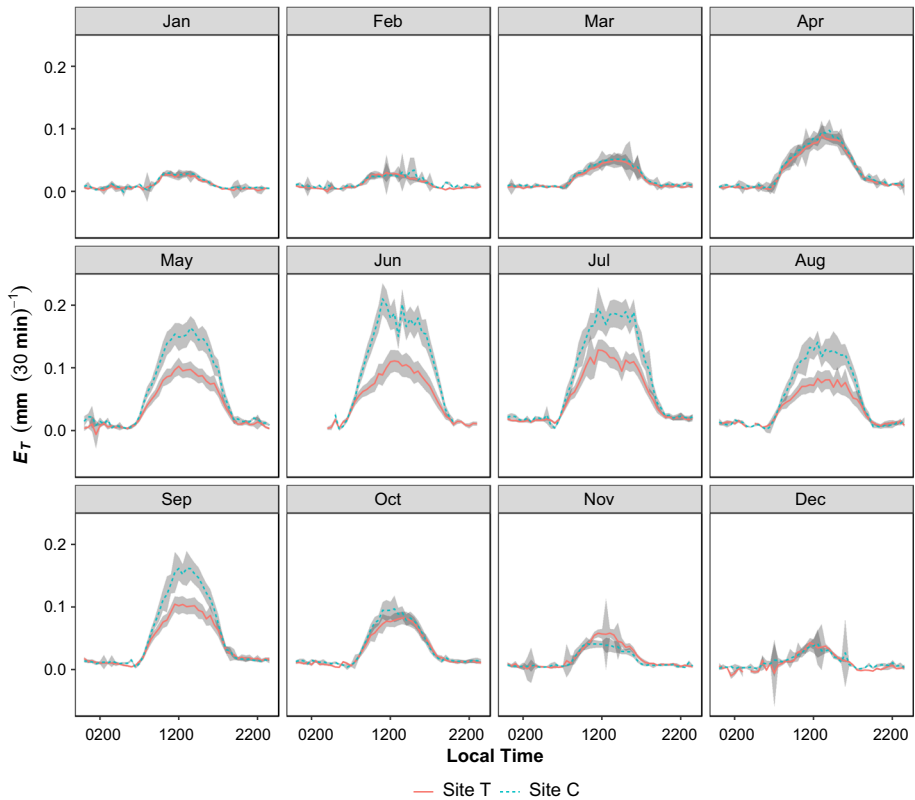


Fig. 8 Diurnal evapotranspiration during each month for the two sites. The curves represent binned ensemble means of measured evapotranspiration values (without gap-filling) at that site for the entire month with the 95% confidence interval (grey shaded ribbons) only from the uncertainty in the random sampling (the larger uncertainties reflect less data availability for those times)

evapotranspiration at Site C was more decoupled from the near-surface atmosphere and more controlled by vegetation physiological processes, which are regulated by the net radiation. However, during the height of the drought (13–24 August, with $\theta_{30} < 0.17 \text{ m}^3 \text{ m}^{-3}$), the mean daytime value of g_s at Site C fell below 10 mm s^{-1} , approaching the concurrently low levels at Site T, and the value of Ω fell below 0.5 for both sites, indicating a strong and similar coupling with the ambient atmosphere for both sites during the drought stress.

5 Discussion

5.1 Soil Heat Storage and Energy-Balance Closure

Because the magnitude of the soil heat storage S_{soil} increases as the vegetation height (or cover) declines (Ochsner et al. 2007), S_{soil} is indispensable for accurate quantification of the ground surface heat flux for areas with low vegetation (Foken 2008). Going beyond several studies that reported the value of S_{soil} could be as large as the sub-surface heat flux (Heusinkveld et al. 2004; Foken 2008; Russell et al. 2015), we reveal that the magnitude of

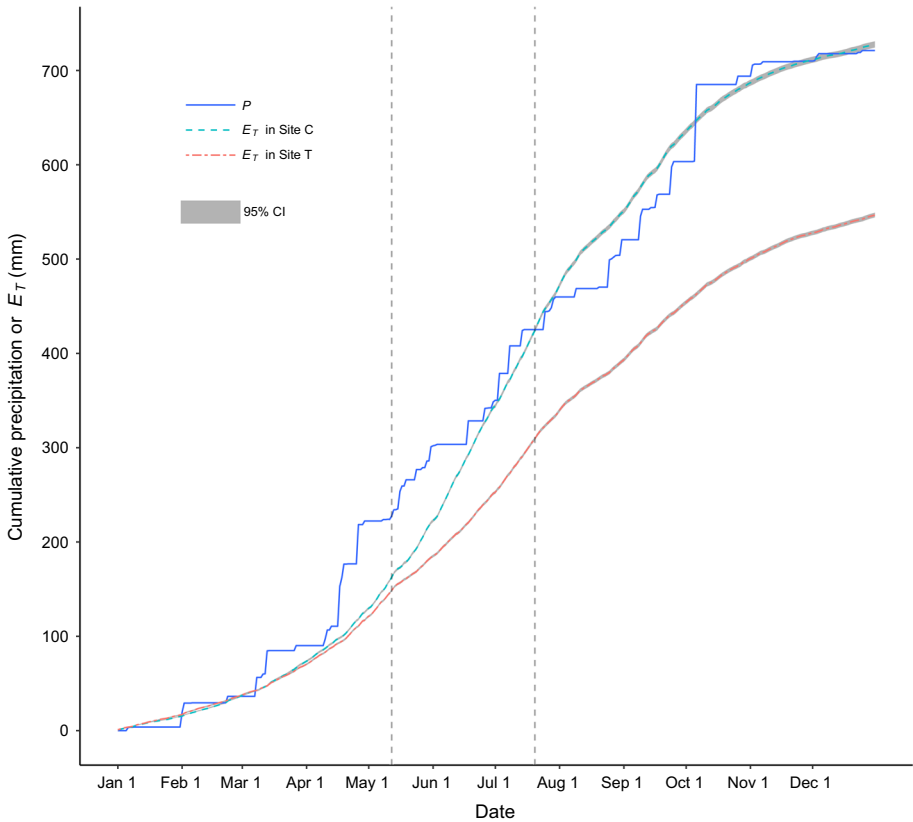


Fig. 9 Comparison of cumulative precipitation with cumulative evapotranspiration for the two sites. The two vertical dashed lines represent the dates of herbicide application. The narrow shaded areas surrounding the cumulative evapotranspiration data represent the small 95% confidence interval derived from random sampling error and gap-filling uncertainty

S_{soil} could be even greater than the sub-surface heat flux and could regulate the diurnal pattern of ground surface heat flux at both our tallgrass prairie sites. The range of variation (-42.2 to 87.6 W m^{-2}) and typical peak times (between 1130 and 1230 LT) of S_{soil} values at Site C were in reasonable agreement with those found elsewhere. For example, data from a maize crop site in south-west Oklahoma showed that mean value of S_{soil} peaked around 0900 LT at 40 W m^{-2} , and decreasing to -15 W m^{-2} at around 1700 LT (Meyers and Hollinger 2004). In the semi-arid Loess Plateau of north-west China, the value of S_{soil} ranged from -40 to 75 W m^{-2} , with the peak time around 1000 LT (Liang et al. 2017), while at a desert-edge site sparsely vegetated with desert reeds, a range of -50 to 100 W m^{-2} was observed (Li et al. 2014). Thus, omitting the soil heat storage would result in an underestimation of the ground surface heat flux, which would lead to an overestimation of the available energy, and thereby weakening the energy-balance closure (Majozi et al. 2017). Further, ignoring the soil heat storage may cause timing errors or phase differences in the diurnal measurements, which may also reduce the energy-balance closure based on 30-min averages (Ochsner et al. 2007). Another study in rice paddy fields found similar differences between sub-surface heat flux and the ground surface heat flux in terms of both the diurnal patterns and phase lags,

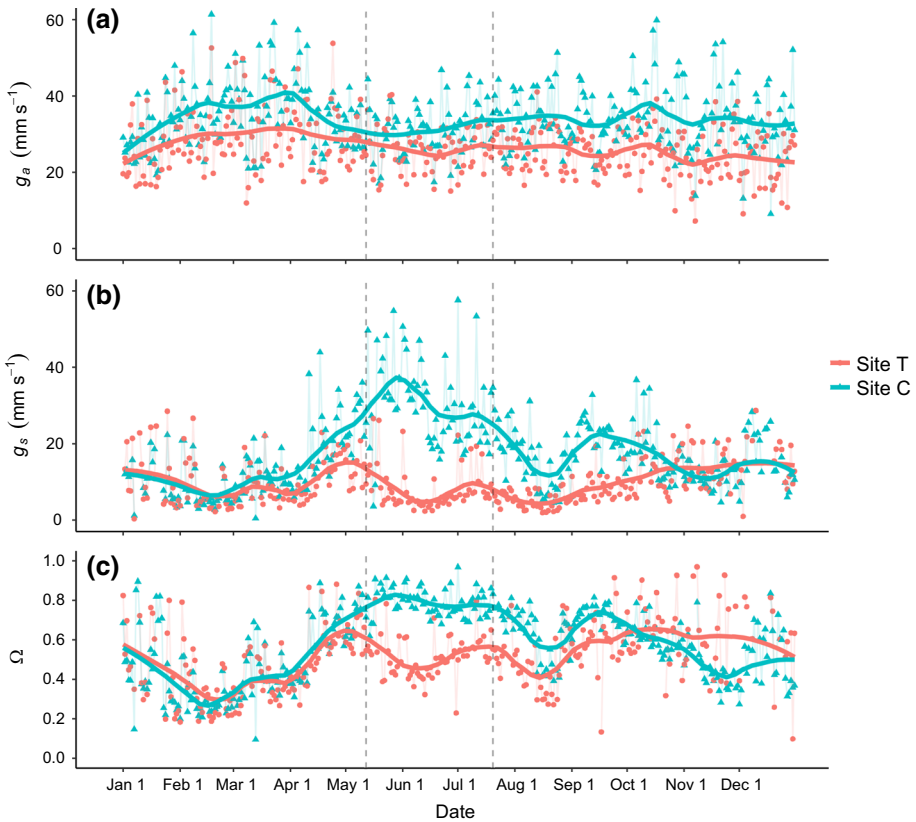


Fig. 10 Variations in aerodynamic conductance (g_a , in **a**), surface conductance (g_s , in **b**), and the decoupling factor (Ω , in **c**) for the two sites. Each point represents the mean daytime (0800–1700 LT) value, and the curves are locally weighted regression regressions with a span of 0.2. The two vertical dashed lines represent the dates of herbicide application

showing an 9% increase in the slope of the energy-balance closure when the value of S_{soil} was considered (Liu et al. 2017). A study on a semi-arid grassland in the Loess Plateau also showed that the integration of S_{soil} into the calculation of the ground surface heat flux increased the budget closure from 76 to 83% (Zuo et al. 2011).

Our yearly energy-balance slopes (0.83 and 0.86) are higher than the value of 0.79 reported by a comprehensive FLUXNET evaluation comprising 22 sites and 50 site-years (Wilson et al. 2002), while the values of the intercepts of 7.8 and 2.8 W m^{-2} at Site T and Site C, respectively, are comparable to the mean intercept of $3.7 \pm 2.0 \text{ W m}^{-2}$ from that study. Another study carried out on a switchgrass field in Chickasha, Oklahoma, during the growing season of 2011, found a closure ratio of 0.77 (Wagle and Kakani 2014), but our closure ratios are better and comparable to the ratio of 0.83 from the same Chickasha site during the growing seasons of 2012 and 2013 (Wagle et al. 2016). Similar closure levels were also reported for other grasslands (Scott 2010; Williams et al. 2012).

However, accurately determining the value of S_{soil} (and thus the value of the ground surface heat flux) at an ecosystem or field scale is problematic for the EC method as heat-flux plates are typically 0.05–0.1 m in diameter and can sample only a tiny area, making it difficult to detect the spatial variability in the soil water content and soil heat storage across a site (Leuning et al. 2012). The high variations in the value of S_{soil} between our two sites exemplified this spatial heterogeneity, which may not have resulted solely from the difference in vegetation coverage. Quantification of the value of ΔT_s , which is the controlling factor in the value of S_{soil} , involves consideration of the active hydrothermal dynamics within this thin soil layer above the heat-flux plates. Many factors related to these hydrothermal processes may contribute to the spatial heterogeneity in the value of S_{soil} , including the surface-cover conditions, the ambient atmosphere, geomorphological characteristics, the soil–water dynamics, and biogeochemical characteristics. Thus, the fact that the measurements of the turbulent and soil heat fluxes are based on different footprints (Wever et al. 2002) may to some degree explain the energy imbalance at both our sites.

A dissimilar footprint is probably not the only cause for the energy imbalance, other factors should be considered as well, including the unmeasured advective fluxes and stationary secondary circulations due to landscape heterogeneity (Foken 2008; Mahr 2010; Foken et al. 2011; Gao et al. 2017). Landscape heterogeneity (engendered by the vegetation treatments) and the consistently higher wind speed at Site T may facilitate the development of strong advection and complicated circulation patterns near the ground, which is a plausible reason for the typically lower monthly closure ratios for Site T. At most of the FLUXNET sites (including those with flat terrain and low vegetation), the energy-balance closure is seldom achieved, but is achievable at homogeneous sites (such as a desert) under all conditions (Foken et al. 2011).

Photosynthesis and canopy storage are consequential factors, and should be accounted for in situations where there is a fully developed tall canopy, such as a maize field (Masseroni et al. 2014). Even in situations where the canopy is typically relatively short, such as at our sites, these energy fluxes can be substantial during the height of the growing season as evidenced by the steady decrease in monthly energy-closure ratios observed at Site C during the middle of the growing season.

In summary, although consideration of the value of S_{soil} considerably increases the magnitude of G_0 and reduces the phase shift, it does not ensure complete energy-balance closure (Cava et al. 2008). Other issues, such as footprint mismatches, landscape heterogeneity, and the canopy heat storage should also be taken into account when attempting to achieve complete energy closure.

5.2 Effects of Active Vegetation on Energy Partitioning

The vegetation treatment produced a divergence in the net radiation R_n between the two sites, being significantly reduced during the summer at Site T, probably because the high reflectance of the grass litter and dead biomass increases the albedo (Wang and Davidson 2007). Li et al. (2000) reported a similar decrease in the value of R_n due to the high albedo for an overgrazed grassland with sparse vegetation coverage. During the growing season, the diurnal variation in the value of G_0 at Site C is positively skewed or peaks in advance of the value of R_n , which is in good agreement with other investigations (Liebethal 2005; Mengelkamp et al. 2006).

During the growing season, the dissipation pattern of available energy showed considerable differences between the two sites as a result of the vegetation treatment. Compared with Site T, the sensible heat flux at Site C is substantially subdued (owing to the shading effect of the leaves) and the latent heat flux is enhanced (because of plant transpiration fed by deeper soil moisture). Similar seasonal patterns of energy partitioning were reported for switchgrass and sorghum fields in Chickasha, Oklahoma (Wagle et al. 2016). At Site C during the peak growing season (June–July), the magnitude of the latent heat flux at midday is roughly double that of the sensible heat flux. This twofold relation was also reported for a mature switchgrass stand in southern Ontario, Canada (Eichelmann et al. 2016). Unlike Site T, a switch in the pattern of the energy partitioning (dominance of the sensible heat flux over the latent heat flux) occurred at Site C during the periods of March–April and October–November (coinciding with the leaf emergence and senescence; see Appendix 1, Fig. 14). A similar concurrence between phenological cycles and a switch in the dominance of the energy fluxes has also been observed in other grassland studies (Ham and Knapp 1998; Wever et al. 2002).

The vegetation treatment at Site T also caused a substantial discrepancy between the two sites in soil water content θ across the profiles, which may alter the divergence in the patterns of energy partitioning between the two sites. The differences in the values of $\theta_{0,3}$ were especially relevant because the highest concentration (70–80%) of the root biomass of these grasses is distributed within the top 0.3 m (Nippert et al. 2012). Compared with Site T, the value of $\theta_{0,3}$ at Site C was substantially reduced during the peak growing season (Fig. 7), during which the value of $\theta_{0,3}$ varied dramatically (between 0.18 and 0.32 $\text{m}^3 \text{m}^{-3}$), but remained above the critical threshold of 0.17 $\text{m}^3 \text{m}^{-3}$. At the same time, the normalized latent heat flux maintained a stable high level (between about 0.60 and 0.75—see Appendix 1, Fig. 15). This steady dominance of the latent heat flux ensured a consistently low Bowen ratio, without regard to the fluctuations in the soil moisture, with similar findings reported for a switchgrass stand in Canada (Eichelmann et al. 2016), and for a temperate grassland in the northern Great Plains (Wever et al. 2002). However, during the severe drought (13–24 August, when the value of $\theta_{0,3}$ at Site C dropped below 0.17 $\text{m}^3 \text{m}^{-3}$), the normalized latent heat flux plunged below 0.5 (between 0.33 and 0.48), approaching the low values observed at Site T for the same period. Because the permanent wilting point of surface soils (within 0.15 m in depth) at Site C is 0.14 $\text{m}^3 \text{m}^{-3}$ given their loam texture (Saxton and Rawls 2006), the drought stress produced when the value of $\theta_{0,3}$ dropped below the critical threshold, and approached the wilting point, substantially suppressing the plant physiological activities. During this drought period, the sensible heat flux became the dominant flux (see Appendix 1, Fig. 15), which agrees with the results from the Oklahoma switchgrass field during a severe drought (Wagle and Kakani 2014). Similar thresholds were also reported from other studies, including 0.15 $\text{m}^3 \text{m}^{-3}$ for a California annual grassland (Baldocchi et al. 2004), 0.14 $\text{m}^3 \text{m}^{-3}$ for a Mediterranean grassland in southern Portugal (Aires et al. 2008), and 0.12 $\text{m}^3 \text{m}^{-3}$ for a tussock grassland in New Zealand (Hunt et al. 2002). An earlier study of native tallgrass prairie in north-central Oklahoma reported that, under conditions of abundant soil moisture, the evaporative fraction (LE/R_n) was controlled by the leaf area index, but when the value of θ fell below a critical threshold, the evaporative fraction instead became controlled by the soil moisture (Burba and Verma 2005). Our study, therefore, has further quantified this critical threshold of soil moisture in the root zone of our study sites.

5.3 Evapotranspiration Dynamics and Soil Water Storage

The seasonal and diurnal patterns of evapotranspiration were typical at both sites. Under the same cumulative precipitation (604 mm) during the growing season, the daily evapotranspiration at Site T ranged between 0.65 and 3.5 mm day⁻¹, with an accumulation of 430 mm, and between 0.55 and 5 mm day⁻¹ at Site C, with an accumulation of 613 mm. By way of comparison, a study done in the native tallgrass prairie of north-central Oklahoma during the growing seasons of 1996–2000 (Burba and Verma 2005) found comparable magnitudes of evapotranspiration (3.5–5 mm day⁻¹), while the study carried out on the switchgrass field in Chickasha, Oklahoma, during the growing seasons of 2011, 2012, and 2013 reported daily evapotranspiration ranges of, respectively, 0.5–4.8, 1.0–6.2, and 1.0–6.7 mm day⁻¹, with accumulations of 450, 653, and 740 mm under cumulative rainfall amounts of 432, 635, and 742 mm (Wagle and Kakani 2014; Wagle et al. 2016). Additionally, the instantaneous maximum at Site C (0.25 mm (30 min)⁻¹) lay between those of the Chickasha site in the dry growing season of 2011 (0.18 mm (30 min)⁻¹) and the wet growing season of 2013 (0.31 mm (30 min)⁻¹) (Wagle and Kakani 2014; Wagle et al. 2016). Similar seasonal trends in evapotranspiration (but lower in magnitude) were also observed at a northern Great Plains site (Wever et al. 2002) and in a switchgrass field in Pennsylvania (Skinner and Adler 2010).

The difference in vegetation cover after treatment brought about dramatic differences in the magnitudes of evapotranspiration as well as differences in soil-moisture variability between the two sites, implying that the presence of active vegetation vitally influences evapotranspiration, and showing the importance of deep soil moisture for plant transpiration. Cumulative evapotranspiration exceeded cumulative precipitation at Site C during the peak growing season (July 21), which was also observed in the Chickasha switchgrass site in two of the three years (Wagle and Kakani 2014). Then, with the arrival of the drought, the grasses at Site C were no longer able to reliably access deep soil water, with the bottom soil layer (0.8-m depth) reaching a stable state of depletion between late August and early October (see Appendix 1, Fig. 12). Clearly, the soil water stored and accumulated prior to the growing season served as an important reservoir for meeting peak evapotranspiration demands during the growing season, as was also reported in other studies (Sun et al. 2011; Valayamkunnath et al. 2018). Once the stored soil water had been exhausted, evapotranspiration became more dependent on precipitation patterns. Because the magnitude of evapotranspiration, and thus the productivity of the ecosystem, are strongly influenced by precipitation patterns and canopy development (Wagle et al. 2016), extreme hydrological events predicted by climate-change scenarios and/or woody plant encroachment may threaten the sustainability of this endangered tallgrass prairie (Fay et al. 2008, 2011; Ge and Zou 2013).

5.4 Environmental and Biological Controls on Surface Conductance

Variations in daily evapotranspiration correspond closely to those of the surface conductance g_s (see Figs. 7, 10), which is more dependent on the soil conductance at Site T, and is thus controlled by the near-surface soil moisture. As shown at Site C, with wet soils, the initial leaf expansion early in the growing season could have contributed to an increase in the value of g_s (Wilson and Baldocchi, 2000). Leaf expansion and the reliable access to deep soil moisture at Site C maintained a greater value of the NDV index and higher g_s values until the end of May, consistent with that observed in the steppe ecosystems of Inner Mongolia, China (Chen et al. 2009). After complete leaf expansion, the value of g_s becomes controlled more by the environmental conditions (Wilson and Baldocchi 2000; Wever et al. 2002). For example, at

Site C, a lower soil moisture and a higher vapour pressure deficit during the two dry intervals in June and August caused decreases in the value of g_s . But the magnitude of g_s at Site C is greater than $10\text{--}25\text{ mm s}^{-1}$, which is reported by an earlier study in the tallgrass prairie (Kim and Verma 1990), possibly due to the wetter soils and consequently higher NDV index during late May and early June at our sites.

The seasonal fluctuation of the decoupling factor Ω above and below 0.5 at Site C was also reported for the steppe ecosystems in Inner Mongolia (Chen et al. 2009), as well as for the annual grassland in California (Ryu et al. 2008). From mid-May to late August, the value of Ω at Site C gradually declined in response to the seasonal leaf development, the reductions in soil moisture, and an increase in the vapour pressure deficit, with similar trends reported by others (Wever et al. 2002; Hao et al. 2007). Furthermore, in the same way as for the trends in the energy partitioning and the normalized latent heat flux, the trends in the values of g_s and Ω are affected by the threshold value of the soil–water content $\theta_{0,3}$ ($0.17\text{ m}^3\text{ m}^{-3}$), which determines the controlling factors for evapotranspiration. Above this threshold, differences in evapotranspiration between the two sites are mainly explained by the differences in vegetation cover, whereas they are more explainable by differences in the value of g_s and the vapour pressure deficit when below the threshold.

6 Summary and Conclusions

To improve understanding of the effect of active vegetation on the energy balance, soil–water dynamics, and the water–vapour exchange between the surface and atmosphere, 1 year observations of the turbulent fluxes and evapotranspiration were collected within two collocated tallgrass prairie sites having contrasting vegetation cover, including a site treated with herbicide spraying and mowing, and a control site left undisturbed. One striking finding of our measurements is the greater importance of the soil heat storage above the heat-flux plates (set at 0.08 m below the ground) than the sub-surface heat flux for quantifying ground surface heat flux, both temporally and in magnitude. Though integration of the soil heat storage is of major importance in calculating the magnitude and temporal phase of the ground surface heat flux for both our sites, the soil heat storage is also highly variable and difficult to quantify because of the active hydrothermal processes within the thin soil layer above the heat-flux plates. The problem of the energy-balance closure at short time scales remains a challenge, and the achievement of an improved closure requires further work on the spatial extrapolation of the soil heat storage, as well as taking into account the error sources due to landscape heterogeneity.

During the growing season, following the removal of active vegetation, the seasonal and diurnal patterns of energy partitioning at the treated site diverged dramatically from those at the control site where the vegetation remained intact. The increase in albedo after the vegetation treatment at the treated site caused a decrease in the net radiation, while the shading effect of the vegetation canopy substantially reduced the magnitude of the sensible heat flux at the control site, with the greater plant transpiration (fed by soil moisture in the root zone) leading to the increase and eventual dominance of the latent heat flux. However, during the severe dry spell in August, the soil water content in the root zone at the control site was depleted below a critical threshold ($0.17\text{ m}^3\text{ m}^{-3}$), resulting in a drought stress, which suppressed plant physiological activities, and brought about a convergence in the energy-partitioning patterns between the two sites.

As for the energy partitioning, the time series of the evapotranspiration flux at the paired sites were similar prior to the treatment, but diverged afterwards, with different meteorological and biological controlling factors coming into play. The active vegetation and higher surface conductance at the control site led to higher rates of evapotranspiration during the early growing season, when net radiation was the controlling factor. With the gradual depletion of soil moisture to below the critical threshold, the vegetation underwent drought suppression, substantially reducing the latent heat flux and evapotranspiration, so that the vapour pressure deficit and surface conductance became the constraining factors. Thus, the canopy growth and soil water availability are two crucial factors in modulating the energy partitioning, surface conductance, and evapotranspiration. Clearly, any land-cover change or vegetation-management action that alters these two factors, such as woody plant encroachment, may significantly alter the energy and water budgets in the endangered tallgrass prairie.

Acknowledgements We are grateful for the insightful comments from the two anonymous reviewers. This research was funded by the National Science Foundation's Dynamics of Coupled Natural and Human Systems (CNH) program (DEB-1413900). Xiangmin Sun is a PhD student supported by the Sid Kyle Graduate Merit Assistantships in the Department of Ecosystem Science and Management at Texas A&M University. The authors would like to thank Chris Stansberry and Jay Prater for their excellent management of the research site. We also express our appreciation to Georgios Xenakis for his development of the FREddyPro package and for correspondence with the authors. The authors gratefully acknowledge many useful comments provided by James Heilman. We are deeply appreciative of the technical support provided by James Kathilankal, Jiahong Li, and George G. Burba from LI-COR Biosciences, Inc.; and by Sasha Ivans and Ben Conrad from Campbell Scientific, Inc. Finally, the authors are grateful to the many graduate students who helped with field trips, including Briana Wyatt, Patricia Torquato, Giovanna Serrau, Sumit Sharma, and Cynthia Wright.

Appendix 1: Analytical Results

The following figures show further results on the prevailing wind direction, soil–water dynamics across the soil profile, the phase shifts between the two components of the ground surface heat flux heat flux G_0 , average monthly energy partitioning, and seasonal variations in the normalized sensible and latent heat fluxes (Figs. 11, 12, 13, 14, 15).

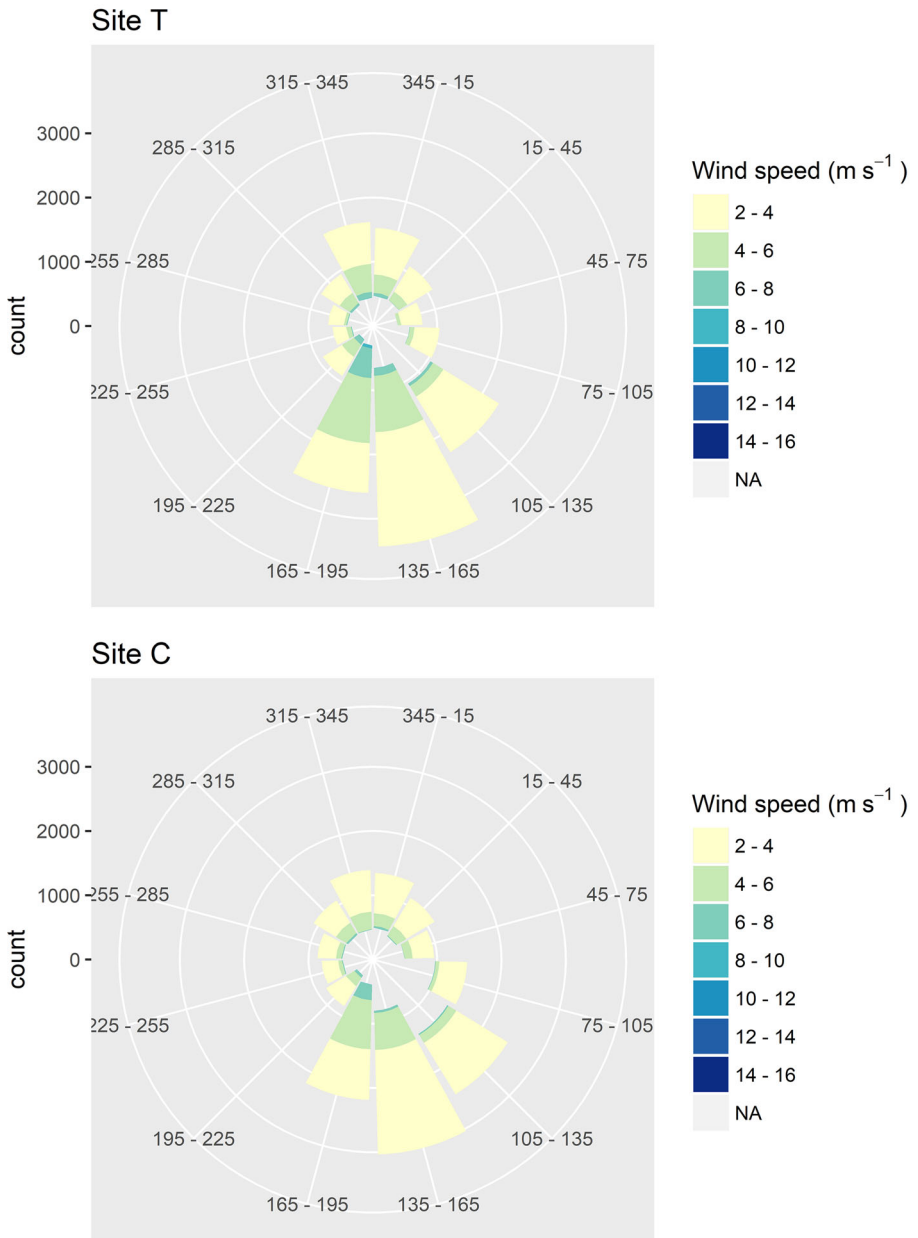


Fig. 11 Wind rose maps for the two sites

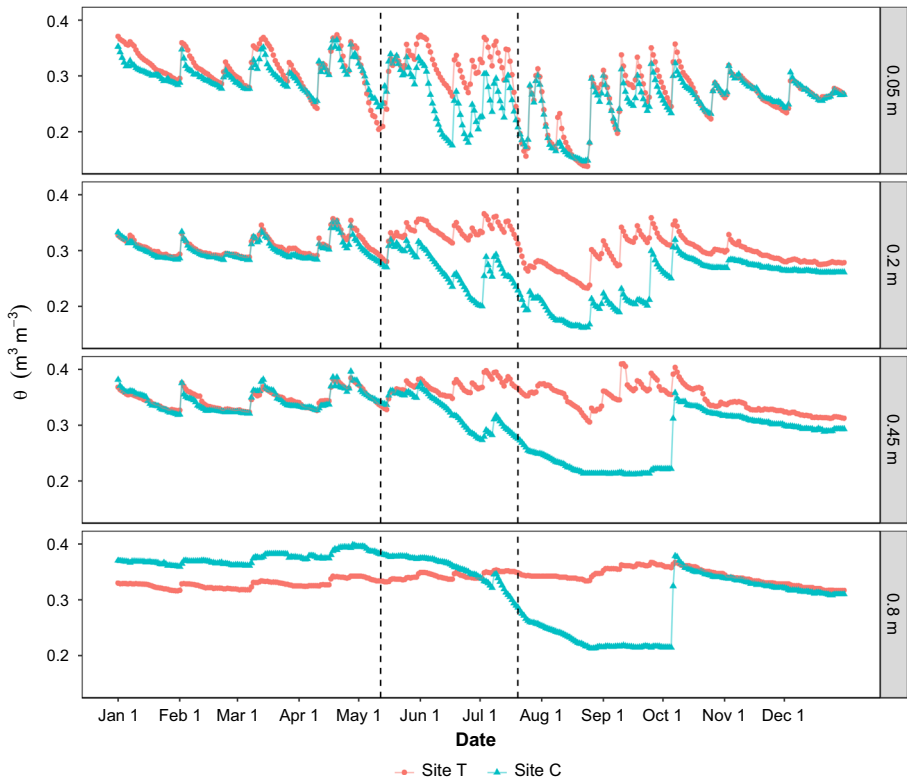


Fig. 12 Dynamics of volumetric soil moisture (θ) across the soil profiles at the two sites as measured at four depths—0.05, 0.20, 0.45, and 0.80 m—representing, respectively, the soil–water dynamics for the four depth intervals 0–0.1 m, 0.1–0.3 m, 0.3–0.6 m, and 0.6–1.0 m. Each point represents the daily mean value of θ from two measuring stations within each site. Dashed lines indicate the dates of the herbicide treatment

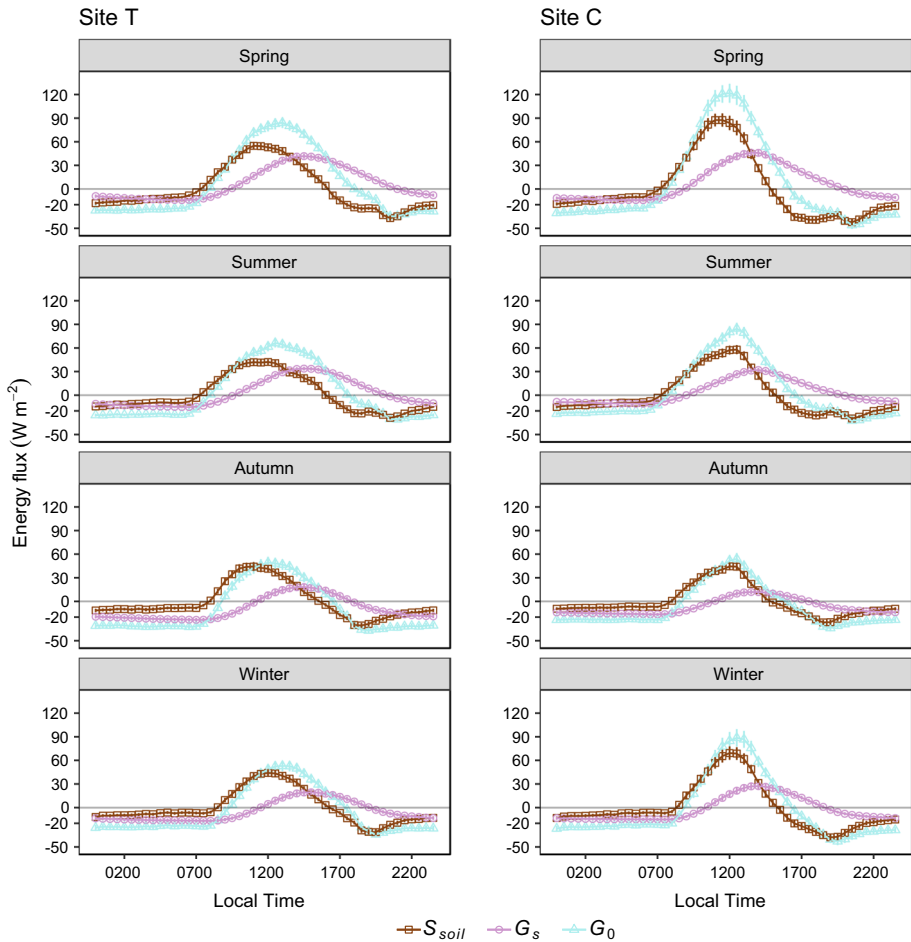


Fig. 13 Diurnal variation of the ground surface heat flux (G_0) and its two components (S_{soil} and G_s) during the different seasons for each site: spring (21 March–20 June), summer (21 June–20 September), autumn (21 September–20 December), and winter (21 December–20 March). Each point is a 30-min ensemble mean for its corresponding flux during that entire season with a 95% confidence interval. Negative values represent the upwards diffusion of heat lost from the surface, and positive values represent the downwards absorption through the ground

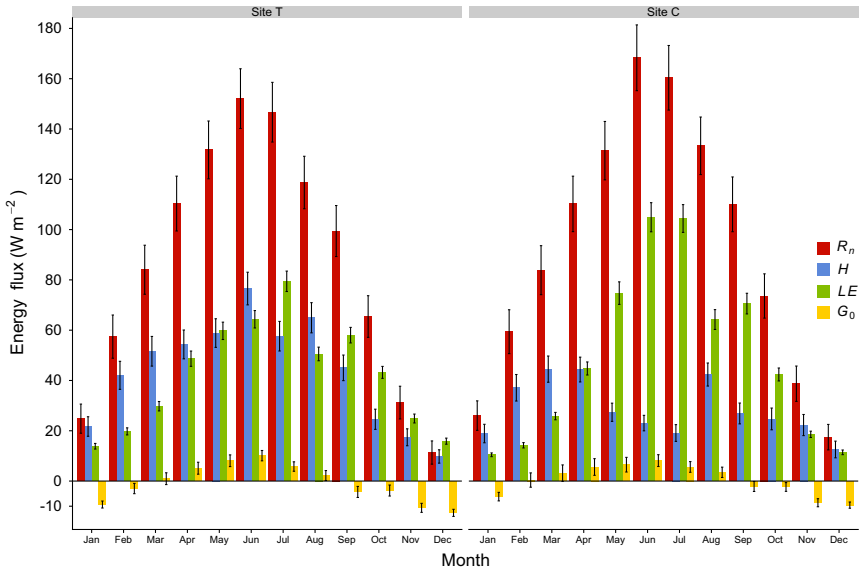


Fig. 14 Monthly means of all energy and turbulent fluxes (R_n , H , LE , and G_0) for the two sites. The bars on each column represent the 95% confidence intervals

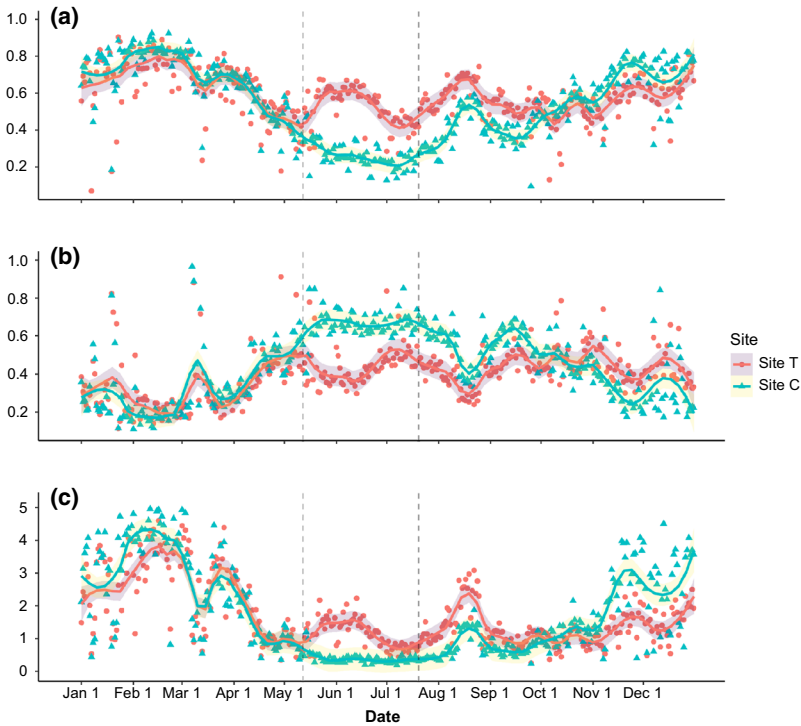


Fig. 15 Variations in daily sensible (a) and latent heat (b) fluxes normalized by the available energy and Bowen ratios (c). Each point in the normalized value and Bowen ratio represents the daytime average when the global radiation is higher than 20 W m^{-2} . All three series were smoothed by a locally weighted regression with a span of 0.1. The two vertical dashed lines represent the dates of herbicide application

Appendix 2: Code Availability

The sample R code for extracting the planetary boundary-layer height based on the geographical location from the North American Regional Reanalysis data is available as open source from the first author's GitHub webpage at https://github.com/sunxm19/Planetary_boundary_height_for_FFP.

References

- Aires LM, Pio CA, Pereira JS (2008) The effect of drought on energy and water vapour exchange above a mediterranean C3/C4 grassland in Southern Portugal. *Agric For Meteorol* 148(4):565–579
- Ammann C, Flechard CR, Leifeld J, Neftel A, Fuhrer J (2007) The carbon budget of newly established temperate grassland depends on management intensity. *Agr Ecosyst Environ* 121(1–2):5–20
- Anderson RG, Wang D (2014) Energy budget closure observed in paired Eddy covariance towers with increased and continuous daily turbulence. *Agric For Meteorol* 184:204–209

- Arnold KB (2010) Eddy covariance in a tallgrass prairie: energy balance closure, water and carbon budgets, and shrub expansion. Kansas State University, Kansas
- Baldocchi DD (2003) Assessing the eddy covariance technique for evaluating carbon dioxide exchange rates of ecosystems: past, present and future. *Global Change Biol* 9(4):479–492
- Baldocchi D, Falge E, Gu LH, Olson R, Hollinger D, Running S, Anthoni P, Bernhofer C, Davis K, Evans R, Fuentes J, Goldstein A, Katul G, Law B, Lee XH, Malhi Y, Meyers T, Munger W, Oechel W, Pilegaard K, Schmid HP, Valentini R, Verma S, Vesala T, Wilson K, Wofsy S (2001) FLUXNET: a new tool to study the temporal and spatial variability of ecosystem-scale carbon dioxide, water vapor, and energy flux densities. *Bull Am Meteorol Soc* 82(11):2415–2434
- Baldocchi DD, Xu LK, Kiang N (2004) How plant functional-type, weather, seasonal drought, and soil physical properties alter water and energy fluxes of an oak-grass savanna and an annual grassland. *Agric For Meteorol* 123(1–2):13–39
- Boval M, Dixon RM (2012) The importance of grasslands for animal production and other functions: a review on management and methodological progress in the tropics. *Animal* 6(5):748–762
- Bremer DJ, Ham JM (1999) Effect of spring burning on the surface energy balance in a tallgrass prairie. *Agric For Meteorol* 97(1):43–54
- Brock FV, Crawford KC, Elliott RL, Cuperus GW, Stadler SJ, Johnson HL, Eilts MD (1995) The Oklahoma Mesonet—a technical overview. *J Atmos Ocean Technol* 12(1):5–19
- Burba G (2013) Eddy covariance method for scientific, industrial, agricultural and regulatory applications: a field book on measuring ecosystem gas exchange and areal emission rates. LI-Cor Biosciences
- Burba GG, Verma SB (2005) Seasonal and interannual variability in evapotranspiration of native tallgrass prairie and cultivated wheat ecosystems. *Agric For Meteorol* 135(1–4):190–201
- Campbell Scientific I (2016) Model HFP01 soil heat flux plate, instruction manual, pp 5–6
- Cava D, Contini D, Donato A, Martano P (2008) Analysis of short-term closure of the surface energy balance above short vegetation. *Agric For Meteorol* 148(1):82–93
- Chen SP, Chen JQ, Lin GH, Zhang WL, Miao HX, Wei L, Huang JH, Han XG (2009) Energy balance and partition in Inner Mongolia steppe ecosystems with different land use types. *Agric For Meteorol* 149(11):1800–1809
- Conant S, Risser PG (1974) Canopy structure of a tall-grass prairie. *J Range Manage* 27(4):313–318
- Eder F, De Roo F, Rotenberg E, Yakir D, Schmid HP, Mauder M (2015) Secondary circulations at a solitary forest surrounded by semi-arid shrubland and their impact on eddy-covariance measurements. *Agric For Meteorol* 211:115–127
- Eichelmann E, Wagner-Riddle C, Warland J, Deen B, Voroney P (2016) Evapotranspiration, water use efficiency, and energy partitioning of a mature switchgrass stand. *Agric For Meteorol* 217:108–119
- Fay PA, Kaufman DM, Nippert JB, Carlisle JD, Harper CW (2008) Changes in grassland ecosystem function due to extreme rainfall events: implications for responses to climate change. *Global Change Biol* 14(7):1600–1608
- Fay PA, Blair JM, Smith MD, Nippert JB, Carlisle JD, Knapp AK (2011) Relative effects of precipitation variability and warming on tallgrass prairie ecosystem function. *Biogeosciences* 8(10):3053–3068
- Finkelstein PL, Sims PF (2001) Sampling error in eddy correlation flux measurements. *J Geophys Res Atmos* 106(D4):3503–3509
- Fischer ML, Torn MS, Billesbach DP, Doyle G, Northup B, Biraud SC (2012) Carbon, water, and heat flux responses to experimental burning and drought in a tallgrass prairie. *Agric For Meteorol* 166:169–174
- Foken T (1998) Die scheinbar ungeschlossene Energiebilanz am Erdboden—eine Herausforderung an die Experimentelle Meteorologie. *Sitzungsberichte der Leibniz-Sozietät* 24(5):131–150
- Foken T (2008) The energy balance closure problem: an overview. *Ecol Appl* 18(6):1351–1367
- Foken T, Göckede M, Mauder M, Mahrt L, Amiro B, Munger W (2004) Post-field data quality control, handbook of micrometeorology. Springer, Berlin
- Foken T, Aubinet M, Finnigan JJ, Leclerc MY, Mauder M, Kyaw Tha Paw U (2011) Results of a panel discussion about the energy balance closure correction for trace gases. *Bull Am Meteorol Soc* 92(4):18
- Frank JM, Massman WJ, Ewers BE (2013) Underestimates of sensible heat flux due to vertical velocity measurement errors in non-orthogonal sonic anemometers. *Agric For Meteorol* 171:72–81
- Franssen HJH, Stockli R, Lehner I, Rotenberg E, Seneviratne SI (2010) Energy balance closure of eddy-covariance data: a multisite analysis for European FLUXNET stations. *Agric For Meteorol* 150(12):1553–1567
- Gao ZM, Liu HP, Katul GG, Foken T (2017) Non-closure of the surface energy balance explained by phase difference between vertical velocity and scalars of large atmospheric eddies. *Environ Res Lett* 12(3):034025
- Ge JJ, Zou C (2013) Impacts of woody plant encroachment on regional climate in the southern Great Plains of the United States. *J Geophys Res Atmos* 118(16):9093–9104

- Ham JM, Knapp AK (1998) Fluxes of CO₂, water vapor, and energy from a prairie ecosystem during the seasonal transition from carbon sink to carbon source. *Agric For Meteorol* 89(1):1–14
- Hao YB, Wang YF, Huang XZ, Cui XY, Zhou XQ, Wang SP, Niu HS, Jiang GM (2007) Seasonal and interannual variation in water vapor and energy exchange over a typical steppe in Inner Mongolia, China. *Agric For Meteorol* 146(1–2):57–69
- Heidbach K, Schmid HP, Mauder M (2017) Experimental evaluation of flux footprint models. *Agric For Meteorol* 246:142–153
- Heusinkveld BG, Jacobs AFG, Aam H, Berkowicz SM (2004) Surface energy balance closure in an arid region: role of soil heat flux. *Agric For Meteorol* 122(1–2):21–37
- Horst TW, Semmer SR, Maclean G (2015) Correction of a non-orthogonal, three-component sonic anemometer for flow distortion by transducer shadowing. *Boundary-Layer Meteorol* 155(3):371–395
- Hunt JE, Kelliher FM, Mcseveny TM, Byers JN (2002) Evaporation and carbon dioxide exchange between the atmosphere and a tussock grassland during a summer drought. *Agric For Meteorol* 111(1):65–82
- Jarvis PG, Mcnaughton KG (1986) Stomatal control of transpiration—scaling up from leaf to region. *Adv Ecol Res* 15:1–49
- Katul GG, Oren R, Manzoni S, Higgins C, Parlange MB (2012) Evapotranspiration: a process driving mass transport and energy exchange in the soil-plant-atmosphere-climate system. *Rev Geophys*. <https://doi.org/10.1029/2011RG000366>
- Kidston J, Brummer C, Black TA, Morgenstern K, Nestic Z, Mccaughey JH, Barr AG (2010) Energy balance closure using Eddy covariance above two different land surfaces and implications for CO₂ flux measurements. *Boundary-Layer Meteorol* 136(2):193–218
- Kim J, Verma SB (1990) Components of surface energy balance in a temperate grassland ecosystem. *Boundary-Layer Meteorol* 51(4):401–417
- Kljun N, Calanca P, Rotach MW, Schmid HP (2004) A simple parameterisation for flux footprint predictions. *Boundary-Layer Meteorol* 112(3):503–523
- Kljun N, Calanca P, Rotach MW, Schmid HP (2015) A simple two-dimensional parameterisation for flux footprint prediction (FFP). *Geosci Model Dev*. 8(11):3695–3713
- Knapp AK, Smith MD (2001) Variation among biomes in temporal dynamics of aboveground primary production. *Science* 291(5503):481–484
- Kochendorfer J, Meyers TP, Frank J, Massman WJ, Heuer MW (2012) How well can we measure the vertical wind speed? Implications for fluxes of energy and mass. *Boundary-Layer Meteorol* 145(2):383–398
- Kosugi Y, Takanashi S, Tanaka H, Ohkubo S, Tani M, Yano M, Katayama T (2007) Evapotranspiration over a Japanese cypress forest. I. Eddy covariance fluxes and surface conductance characteristics for 3 years. *J Hydrol* 337(3–4):269–283
- Leuning R, Van Gorsel E, Massman WJ, Isaac PR (2012) Reflections on the surface energy imbalance problem. *Agric For Meteorol* 156:65–74
- Li SG, Harazono Y, Oikawa T, Zhao HL, He ZY, Chang XL (2000) Grassland desertification by grazing and the resulting micrometeorological changes in Inner Mongolia. *Agric For Meteorol* 102(2–3):125–137
- Li Y, Liu SH, Wang S, Miao YC, Chen BC (2014) Comparative study on methods for computing soil heat storage and energy balance in arid and semi-arid areas. *J Meteorol Res* 28(2):308–322
- Liang JN, Zhang L, Cao XJ, Wen J, Wang JM, Wang GY (2017) Energy balance in the semiarid area of the Loess Plateau, China. *J Geophys Res Atmos* 122(4):2155–2168
- Liebenthal C (2005) On the determination of the ground heat flux in micrometeorology and its influence on the energy balance closure. Doctoral dissertation
- Limb RF, Engle DM, Alford AL, Hellgren EC (2010) Tallgrass prairie plant community dynamics along a canopy cover gradient of eastern redcedar (*Juniperus virginiana* L.). *Rangel Ecol Manag* 63(6):638–644
- Liu XY, Yang SH, Xu JZ, Zhang JG, Liu JT (2017) Effects of soil heat storage and phase shift correction on energy balance closure of paddy fields. *Atmosfera* 30(1):39–52
- Mahrt L (2010) Computing turbulent fluxes near the surface: needed improvements. *Agric For Meteorol* 150(4):501–509
- Majozzi NP, Mannaerts CM, Ramoelo A, Mathieu R, Nickless A, Verhoef W (2017) Analysing surface energy balance closure and partitioning over a semi-arid savanna FLUXNET site in Skukuza, Kruger National Park, South Africa. *Hydrol Earth Syst Sci* 21(7):3401–3415
- Masseroni D, Corbari C, Mancini M (2014) Limitations and improvements of the energy balance closure with reference to experimental data measured over a maize field. *Atmosfera* 27(4):335–352
- Mauder M, Foken T (2006) Impact of post-field data processing on eddy covariance flux estimates and energy balance closure. *Meteorol Z* 15(6):597–609
- Mckinley DC, Blair JM (2008) Woody plant encroachment by *Juniperus virginiana* in a mesic native grassland promotes rapid carbon and nitrogen accrual. *Ecosystems* 11(3):454–468

- McPherson RA, Fiebrich CA, Crawford KC, Elliott RL, Kilby JR, Grimsley DL, Martinez JE, Basara JB, Illston BG, Morris DA, Kloesel KA, Stadler SJ, Melvin AD, Sutherland AJ, Shrivastava H, Carlson JD, Wolfenbarger JM, Bostic JP, Demko DB (2007) Statewide monitoring of the mesoscale environment: a technical update on the Oklahoma Mesonet. *J Atmos Ocean Technol* 24(3):301–321
- Mengelkamp HT, Beyrich F, Heinemann G, Ament F, Bange J, Berger F, Bosenberg J, Foken T, Hennemuth B, Heret C, Huneke S, Johnsen KP, Kerschgens M, Kohsiek W, Leps JP, Liebthal C, Lohse H, Mauder M, Meijninger W, Raasch S, Simmer C, Spiess T, Tittebrand A, Uhlenbrock J, Zittel R (2006) Evaporation over a heterogeneous land surface—the EVA-GRIPS project. *Bull Am Meteorol Soc* 87(6):775–786
- Mesonet (2016) Mesonet long-term averages—maps. https://www.mesonet.org/index.php/weather/mesonet_averages_maps#y=average&m=ann&p=rnet_sm&d=false
- Meyers TP (2001) A comparison of summertime water and CO₂ fluxes over rangeland for well watered and drought conditions. *Agric For Meteorol* 106(3):205–214
- Meyers TP, Hollinger SE (2004) An assessment of storage terms in the surface energy balance of maize and soybean. *Agric For Meteorol* 125(1–2):105–115
- Moncrieff JB, Massheder JM, De Bruin H, Elbers J, Friborg T, Heusinkveld B, Kabat P, Scott S, Soegaard H, Verhoef A (1997) A system to measure surface fluxes of momentum, sensible heat, water vapour and carbon dioxide. *J Hydrol* 188:589–611
- Moncrieff J, Clement R, Finnigan J, Meyers T (2005) Averaging, detrending, and filtering of Eddy covariance time series. In: Lee X, Massman W, Law B (eds) *Handbook of micrometeorology: a guide for surface flux measurement and analysis*. Springer, Dordrecht
- Monteith J (1965) The state and movement of water in living organisms. In: *Proceedings of evaporation and environment, XIXth Symposium 1965*, pp 205–234
- Monteith JL, Unsworth MH (2013) *Principles of environmental physics: plants, animals, and the atmosphere*. Elsevier, Amsterdam
- Moritz S, Sardá A, Bartz-Beielstein T, Zaefferer M, Stork J (2015) Comparison of different methods for univariate time series imputation in R. *arXiv preprint arXiv:151003924*
- Nippert JB, Wieme RA, Ocheltree TW, Craine JM (2012) Root characteristics of C-4 grasses limit reliance on deep soil water in tallgrass prairie. *Plant Soil* 355(1–2):385–394
- Novick KA, Oren R, Stoy PC, Siqueira MBS, Katul GG (2009) Nocturnal evapotranspiration in eddy-covariance records from three co-located ecosystems in the Southeastern US: implications for annual fluxes. *Agric For Meteorol* 149(9):1491–1504
- Ochsner TE, Sauer TJ, Horton R (2007) Soil heat storage measurements in energy balance studies. *Agron J* 99(1):311–319
- O'mara FP (2012) The role of grasslands in food security and climate change. *Ann Bot* 110(6):1263–1270
- Oncley SP, Foken T, Vogt R, Kohsiek W, Debruin HAR, Bernhofer C, Christen A, Van Gorsel E, Grantz D, Feigenwinter C, Lehner I, Liebthal C, Liu H, Mauder M, Pitacco A, Ribeiro L, Weidinger T (2007) The energy balance experiment EBEX-2000. Part I: overview and energy balance. *Boundary-Layer Meteorol* 123(1):1–28
- Papale D, Reichstein M, Aubinet M, Canfora E, Bernhofer C, Kutsch W, Longdoz B, Rambal S, Valentini R, Vesala T, Yakir D (2006) Towards a standardized processing of net ecosystem exchange measured with eddy covariance technique: algorithms and uncertainty estimation. *Biogeosciences* 3(4):571–583
- Reichstein M, Falge E, Baldocchi D, Papale D, Aubinet M, Berbigier P, Bernhofer C, Buchmann N, Gilmanov T, Granier A, Grunwald T, Havrankova K, Ilvesniemi H, Janous D, Knohl A, Laurila T, Lohila A, Loustau D, Matteucci G, Meyers T, Miglietta F, Ourcival JM, Pumpanen J, Rambal S, Rotenberg E, Sanz M, Tenhunen J, Seufert G, Vaccari F, Vesala T, Yakir D, Valentini R (2005) On the separation of net ecosystem exchange into assimilation and ecosystem respiration: review and improved algorithm. *Global Change Biol* 11(9):1424–1439
- Ricketts TH (1999) *Terrestrial ecoregions of North America: a conservation assessment*. Island Press, Washington, DC
- Russell ES, Liu HP, Gao ZM, Finn D, Lamb B (2015) Impacts of soil heat flux calculation methods on the surface energy balance closure. *Agric For Meteorol* 214:189–200
- Ryu Y, Baldocchi DD, Ma S, Hehn T (2008) Interannual variability of evapotranspiration and energy exchange over an annual grassland in California. *J Geophys Res Atmos*. <https://doi.org/10.1029/2007JD009263>
- Samson FB, Knopf FL, Ostlie WR (2004) Great Plains ecosystems: past, present, and future. *Wildl Soc Bull* 32(1):6–15
- Saxton KE, Rawls WJ (2006) Soil water characteristic estimates by texture and organic matter for hydrologic solutions. *Soil Sci Soc Am J* 70(5):1569–1578
- Schulze ED, Kelliher FM, Korner C, Lloyd J, Leuning R (1994) Relationships among maximum stomatal conductance, ecosystem surface conductance, carbon assimilation rate, and plant nitrogen nutrition—a global ecology scaling exercise. *Annu Rev Ecol Syst* 25:629–662

- Scott RL (2010) Using watershed water balance to evaluate the accuracy of eddy covariance evaporation measurements for three semiarid ecosystems. *Agric For Meteorol* 150(2):219–225
- Scott RL, Huxman TE, Barron-Gafford GA, Jenerette GD, Young JM, Hamerlynck EP (2014) When vegetation change alters ecosystem water availability. *Global Change Biol.* 20(7):2198–2210
- Skinner RH, Adler PR (2010) Carbon dioxide and water fluxes from switchgrass managed for bioenergy production. *Agr Ecosyst Environ* 138(3–4):257–264
- Stoy PC, Mauder M, Foken T, Marcolla B, Boegh E, Ibrom A, Arain MA, Arneth A, Aurela M, Bernhofer C, Cescatti A, Dellwik E, Duce P, Gianelle D, Van Gorsel E, Kiely G, Knohl A, Margolis H, Mccaughey H, Merbold L, Montagnani L, Papale D, Reichstein M, Saunders M, Serrano-Ortiz P, Sottocornola M, Spano D, Vaccari F, Varlagin A (2013) A data-driven analysis of energy balance closure across FLUXNET research sites: the role of landscape scale heterogeneity. *Agric For Meteorol* 171:137–152
- Sun G, Alstad K, Chen JQ, Chen SP, Ford CR, Lin GH, Liu CF, Lu N, McNulty SG, Miao HX, Noormets A, Vose JM, Wilske B, Zeppel M, Zhang Y, Zhang ZQ (2011) A general predictive model for estimating monthly ecosystem evapotranspiration. *Ecohydrology* 4(2):245–255
- Twine TE, Kustas WP, Norman JM, Cook DR, Houser PR, Meyers TP, Prueger JH, Starks PJ, Wesely ML (2000) Correcting eddy-covariance flux underestimates over a grassland. *Agric For Meteorol* 103(3):279–300
- Tyrl RJ, Bidwell TG, Masters RE, Elmore RD, Weir JR (2007) Oklahoma's native vegetation types, Oklahoma State University, Oklahoma Cooperative Extension Service, Stillwater, OK, USA, p. 8
- Valayamkunnath P, Sridhar V, Zhao W, Allen RG (2018) Intercomparison of surface energy fluxes, soil moisture, and evapotranspiration from eddy covariance, large-aperture scintillometer, and modeling across three ecosystems in a semiarid climate. *Agric For Meteorol* 248:22–47
- Vickers D, Mahrt L (1997) Quality control and flux sampling problems for tower and aircraft data. *J Atmos Ocean Technol* 14(3):512–526
- Wagle P, Kakani VG (2014) Growing season variability in evapotranspiration, ecosystem water use efficiency, and energy partitioning in switchgrass. *Ecohydrology* 7(1):64–72
- Wagle P, Kakani VG, Huhnke RL (2016) Evapotranspiration and ecosystem water use efficiency of switchgrass and high biomass sorghum. *Agron J* 108(3):1007–1019
- Wang SS, Davidson A (2007) Impact of climate variations on surface albedo of a temperate grassland. *Agric For Meteorol* 142(2–4):133–142
- Web Soil Survey (2003) United States Department of Agriculture. <https://websoilsurvey.sc.egov.usda.gov/ApWebSoilSurvey.aspx>. Cited 01/06/2017
- Webb EK, Pearman GI, Leuning R (1980) Correction of flux measurements for density effects due to heat and water-vapor transfer. *Q J R Meteorol Soc* 106(447):85–100
- Wever LA, Flanagan LB, Carlson PJ (2002) Seasonal and interannual variation in evapotranspiration, energy balance and surface conductance in a northern temperate grassland. *Agric For Meteorol* 112(1):31–49
- Wilczak JM, Oncley SP, Stage SA (2001) Sonic anemometer tilt correction algorithms. *Boundary-Layer Meteorol* 99(1):127–150
- Williams CA, Reichstein M, Buchmann N, Baldocchi D, Beer C, Schwalm C, Wohlfahrt G, Hasler N, Bernhofer C, Foken T, Papale D, Schymanski S, Schaefer K (2012) Climate and vegetation controls on the surface water balance: Synthesis of evapotranspiration measured across a global network of flux towers. *Water Resour Res.* <https://doi.org/10.1029/2011WR011586>
- Wilson KB, Baldocchi DD (2000) Seasonal and interannual variability of energy fluxes over a broadleaved temperate deciduous forest in North America. *Agric For Meteorol* 100(1):1–18
- Wilson K, Goldstein A, Falge E, Aubinet M, Baldocchi D, Berbigier P, Bernhofer C, Ceulemans R, Dolman H, Field C, Grelle A, Ibrom A, Law BE, Kowalski A, Meyers T, Moncrieff J, Monson R, Oechel W, Tenhunen J, Valentini R, Verma S (2002) Energy balance closure at FLUXNET sites. *Agric For Meteorol* 113(1–4):223–243
- Wohlfahrt G, Klumpp K, Soussana J-F (2012) Eddy covariance measurements over grasslands, *Eddy Covariance*. Springer, Berlin
- Wutzler T, Lucas-Moffat A, Migliavacca M, Knauer J, Sickel K, Šigut L, Menzer O, Reichstein M (2018) Basic and extensible post-processing of eddy covariance flux data with REdDyProc. *Biogeosci Discuss* 2018:1–39
- Xu K, Metzger S, Desai AR (2017) Surface-atmosphere exchange in a box: space-time resolved storage and net vertical fluxes from tower-based eddy covariance. *Agric For Meteorol* 255:81–91
- Yue P, Zhang Q, Niu SJ, Cheng H, Wang XY (2011) Effects of the soil heat flux estimates on surface energy balance closure over a semi-arid grassland. *Acta Meteorol Sin* 25(6):774–782
- Zou CB, Turton D, Will RE, Fuhlendorf SD, Engle D, Hung J (2010) PS 62-146: estimating watershed level evapotranspiration using water budget method. In: The 95th ESA annual meeting 2010

- Zou CB, Turton DJ, Will RE, Engle DM, Fuhlendorf SD (2014) Alteration of hydrological processes and streamflow with juniper (*Juniperus virginiana*) encroachment in a mesic grassland catchment. *Hydrol Proc* 28(26):6173–6182
- Zuo J-Q, Wang J-M, Huang J-P, Li W, Wang G, Ren H (2011) Estimation of ground heat flux and its impact on the surface energy budget for a semi-arid grassland. *Sci Cold Arid Reg* 3:41–50